A Godunov-type method in Lagrangian coordinates for computing linearly-perturbed spherically-symmetric flows of gas dynamics

Jean-Marie Clarisse

A Godunov-type method in Lagrangian coordinates for computing linearly-perturbed spherically-symmetric flows of gas dynamics

Jean-Marie Clarisse
∗ *CEA Bruyères-le-Châtel, 91297 Arpajon Cedex, France*
Email: jean-marie.clarisse@cea.fr (+33-1-69-26-42-01 / +33-1-69-26-70-94)

Version: December 14, 2007

An explicit Godunov-type method in Lagrangian coordinates is devised for computing three-dimensional linear perturbations about spherical radial flows of gas dynamics. This method relying on a description of the perturbed flow in terms of linear Lagrangian perturbations is an outgrowth of an unpublished work by the author [11] and of the Godunov-type method for multi-material flows in planar symmetry presented in [13]. The principle of a discrete formulation of the geometric conservation law [46] for the motion perturbation is introduced, granting mass conservation at the perturbation level. A practical time-step constraint for the numerical stability of the linear perturbation computation is provided in the case of third-order non-degenerate Runge–Kutta schemes. The scheme numerical capabilities at producing reliable accurate results are demonstrated by computing free-surface deformations of a shell in homogeneous compression and front deformations of a self-similar converging spherical shock wave. The interest of such a perturbation computation approach in hydrodynamic stability studies is examplified in the latter case by obtaining shock-front deformation dynamics results having no precedents with respect to accuracy and perturbation wavelength range.

Key Words: Gas dynamics; Linear hydrodynamic stability; Lagrangian perturbation; curvilinear coordinates; Godunov-type method; simple Riemann solver; geometric conservation law; Rayleigh-Taylor instability; converging spherical shock-wave stability

1. INTRODUCTION

Consider the spherically-symmetric radial flow of some inviscid, non-heat-conducting, immiscible fluids. The equations modeling such a flow — the Euler equations — may be written, in Lagrangian form, as

$$\begin{gathered}\partial_t \mathbf{U} + \partial_m\big[A\,\mathbf{F}(\mathbf{U})\big] = \mathbf{G}(\mathbf{U}), \qquad \partial_t r = u, \\ A = r^2, \quad \mathbf{U} = (\tau,\ u,\ e)^{\top}, \quad \mathbf{F}(\mathbf{U}) = (-u,\ p,\ p\,u)^{\top}, \quad \mathbf{G}(\mathbf{U}) = (0,\ p\,\partial_m A,\ 0)^{\top},\end{gathered} \tag{1}$$

where τ, p, r, u are, respectively, the fluid specific volume, pressure, particle radial coordinate and velocity, $e = \mathcal{E} + u^2/2$ is the total specific energy ($\mathcal{E}$ standing for the specific internal energy), with equations of state of the form $p = P(\tau, \mathcal{E})$ being assumed, and m is the Lagrangian coordinate satisfying the relation $dm = \rho\,A\,dr$, where $\rho = 1/\tau$ denotes the fluid density. The question of the stability of such a flow, when subject to three-dimensional (3D) perturbations of initial or boundary conditions, arises in many instances, ranging from the study of air bubbles in water (*e. g.* see [1]), to that of stars [33].

Stability analyses of fluid flows often start with a linear stability analysis. In situations where the reference flow — the so-called "basic flow" [17] — depends on time, linearizing the Euler equations about such a flow leads to a linear system of partial differential equations (PDEs) for perturbations. The coefficients of this linear system depending on space and time variables, the method of normal modes [17] no longer applies and one has to solve an initial and boundary value problem (IBVP) for the perturbations. Except in rare occasions, solutions to such problems must be obtained numerically. For spherically-symmetric basic flows, the system of linear perturbation 3D PDEs may be reduced to the consideration of systems of 1D PDEs for the perturbation spherical harmonics components. This reduction of the number of independent variables makes the *linear perturbation computation approach* — i. e. the simultaneous computation of the 1D basic flow and of its linear perturbation modal (spherical harmonics) components — especially useful for stability studies of complex flows. Indeed this approach offers decisive advantages, in terms of reduced computational effort and results accuracy, over multi-dimensional (multi-D) computations of perturbed flows at small perturbation amplitudes: cf. [13, Sec. 1] for a brief discussion. In particular multi-D computations of perturbation evolutions suffer in practice severe limitations with respect to achievable accuracy and/or perturbation spectrum range that can be handled, since the necessary spatial sampling of a perturbation is inversely proportional to its characteristic length along each dimension of space.

As an example, the linear perturbation computation approach may be profitably used in laser-driven inertial confinement fusion (ICF) where thermonuclear burn is expected to be achieved for a sufficiently symmetric implosion of a spherical fuel pellet. Hydrodynamic instabilities occurring during the pellet implosion are critical to the success of ICF as they may lead to flow non-uniformities which could forbid the achievement of thermonuclear reaction conditions. The ability of obtaining detailed and accurate linear perturbation responses — both in time and space — of pellet implosions is thus a key element in the design process of an ICF pellet (*e. g.* see [25]). This fact has primarily motivated the present developments in spherical symmetry. Nevertheless the method devised herein could as well be applied to other compressible flows within the inviscid fluid approximation (such as, for example, in the study of sonoluminescence [18]).

Linear perturbation computation methods for spherically-symmetric 1D unsteady basic flows have been previously proposed whether for investigations in gas dynamics [24, 8], astrophysics (*e. g.* see [14]), or in the more specific context of ICF [27, 42, 34]. These earlier works, when dealing with shock waves, relied on 1D artificial viscosity methods and their extensions to linear perturbations. More recently, the linear perturbation computation approach has been the object of a renewed interest within the framework of nonlinear hyperbolic systems of conservation laws: see [23, 22]. These recent works have led to propose linearized numerical fluxes derived from the Roe method [39, 23] or from acoustic solvers [30, 13] in Lagrangian coordinates, hence allowing the construction of Godunov-type methods for computing linear perturbations of gas dynamical flows in slab symmetry [39, 22, 13]. Such linearized fluxes being granted, devising extensions of the above methods to 1D basic flows with other types of symmetry essentially consists in (i) obtaining the proper system of linear perturbation equations in conservative form, and (ii) — as for the basic flow — carrying out, in compliance with the Lagrangian property of the space discretizing grid, discrete approximations of the geometry-dependent terms specific to these equations.

Such an extension to spherically-symmetric radial flows was carried out in an unpublished work of 2001 by the author (now available as [11]) where a Godunov-type method in Lagrangian coordinates based on the linearized Roe method of [39, 23] was detailed. This work relied on the concept of *Lagrangian perturbations* which is classical in hydrodynamics [2, 33] and which provides a systematic and natural way of handling — both at the theoretical and computational levels — geometrically perturbed contact discontinuities, including perturbation shear motions (*e. g.* see [13]). Particular formulations of the perturbation equations in conservative form were introduced — for basic flows with planar or spherical symmetry [11, App. A.1.2 and Sec. 1.2] — by exploiting a reduction of the 2D transverse motion linear perturbation [7]. In that respect, these formulations differed from any previous work on the subject which either used perturbation equations in non conservative form [27, 42, 34, 7, 14, 24, 8], either were restricted to planar symmetry [39, 23, 22]. The discrete approximation of the geometry-dependent terms in the linear perturbation equations for spherical symmetry was also treated by applying the geometric conservation law principle [46] to the motion perturbation [11, Sec. 2.2 and App. D]. As a whole, this work [11] laid the basis for the treatment of gas dynamical flows with nonlinear heat conduction in [4, 5], for the Godunov-type method — in the linear perturbation equation derivation and formulation — of [13], as well as for the consequent developments and applications of the linear perturbation code SILE$\mathfrak{X}$ [4, 12]. It also provided substantial elements (equation formulations, spherical geometry dependent term discretization, test case results) for the subsequent works of [35, 31] based on the alternative linear perturbation definition of [39, 23, 22].

The method presently described for computing linear perturbations of solutions to (1) proceeds from [11, 5] in the same choice of a Lagrangian perturbation description, in the method of derivation and the formulation of the linearized equations, as well as in the principle of applying the geometric conservation law to the motion perturbation. Although focusing on the gas dynamics equations in spherical symmetry, emphasis has been put on providing key elements that could be useful under other assumptions of continuum media mechanics. Hence, in the spirit of [2, 7], the necessary results for establishing linear Lagrangian perturbation equations in *arbitrary curvilinear coordinates* are given regardless of the particular mathematical kind (*e. g.* conservation laws, diffusion equations, etc) of the PDEs satisfied by the flow variables, equation derivations and conservative formulations in spherical or Cartesian (as in [13]) coordinates following as particular cases. Similarly, the principle of a geometric conservation law formulation for the motion perturbation, being independent of a particular numerical method choice, is of general scope. The numerical scheme itself directly draws from the Godunov-type method for multi-material flows, in its method-of-lines variant, proposed in [13, Sec. 3]. Besides, an alternative construction to those of [30, 13] is given for the linearized numerical flux which establishes this flux equivalence with a linearization of a "simple Riemann solver" [19], thus revealing the underlying perturbation wave structure. Favoring a linear perturbation explicit scheme, a numerical stability analysis — lacking in previous works on Godunov-type methods for linear perturbations — is also included, leading to a practical time-step criterion for explicit third-order non-degenerate Runge–Kutta schemes.

The outline of the paper is the following. The linear Lagrangian perturbation equations associated to Eq. (1) are presented and commented in Section 2, their complete derivation as a particular case of results established in curvilinear coordinates being the object of Appendix A. The explicit Godunov-type scheme in its first-order and MUSCL-type variants is then detailed in Section 3, including the linearized numerical flux identification with a linearized simple Riemann solver (Appendix B), the application of the geometric conservation law to the motion perturbation (Appendix C), and the linear perturbation scheme time-step criterion for stability (Appendix D). Finally, the capabilities of the MUSCL-type scheme are assessed in Section 4 for two different kinds of converging flows: one (Section 4.1) corresponds to a shell isentropic compression sharing certain characteristics with ICF pellet implosions [32, 3, 26], the other (Section 4.2) is a self-similar converging spherical shock wave which has been at the heart of converging shock stability studies [9, 48, 10]. In both cases, quantitative perturbation results are achieved by means of systematic spatial grid refinement studies and their accuracy evaluated through comparisons, in the former case, to reference solutions and, in the latter, to the best results available. In doing so, new determinations of shock-front deformation dynamics for high degree spherical harmonics are obtained, thus demonstrating the interest of using the proposed method and more generally the linear perturbation computation approach in investigations of hydrodynamic stability problems.

2. LAGRANGIAN PERTURBATION EQUATIONS FOR LINEAR HYDRODYNAMIC STABILITY ANALYSES

The problem of the linear stability of a particular solution to (1) is classically formulated, in fluid mechanics, in terms of perturbations which, without further assumption, are functions of three space variables and time. These perturbations are sought as solutions of IBVPs provided by: *(a)* a linearized form of the 3D equations of gas dynamics, *(b)* linear perturbations of the boundary conditions satisfied by the basic flow, and *(c)* linear perturbation initial conditions. Various formulations of these IBVPs may be obtained depending on the particular description of the perturbations that is retained: *e. g.* Eulerian or Lagrangian. Here, as in [11, 13], we adopt the *Lagrangian perturbation* description [2, 33]. In the present case, the linear perturbation equations involved in these linear perturbation IBVPs result from (see Appendix A):

1. *The linearization, about the radial basic flow particle trajectories, of the 3D gas dynamics equations written in conservative form for a Lagrangian description of the fluid motion.*

As advocated in [2, 7], this linearization is presently carried out for basic flows with *arbitrary curvilinear trajectories* (Appendix A.2) using an *arbitrary system of Lagrangian coordinates* (provided it complies with the principles of Lagrangian perturbations). As a consequence the different results which are detailed in Appendix A.2 are of most general scope, including the formulation of the linear Lagrangian perturbation of a scalar conservation law (Proposition 5 of Appendix A.2). The equations relevant to radial basic flows with spherical symmetry ensue then as a particular case (Appendix A.3.2).

2. *A Helmholtz decomposition of the orthoradial — or* transverse *— motion perturbation reducing this motion 2D-vector equations to scalar equations for its sole irrotational part.* Such a reduction calls upon specific properties of the spherical coordinate system metric (Appendix A.3.3).

3. *The expansion over the basis of spherical harmonics — in the variables made of the angular coordinates defining the radial basic flow trajectories — of the previously reduced set of equations.* This expansion transforms the 3D partial differential equations (PDEs) for linear perturbations into systems of 1D PDEs, in the variables (m, t), for these perturbation spherical harmonics — termed here *modal* — components (Appendix A.3.4). Moreover, perturbation modal components of identical spherical harmonics degree but distinct orders satisfy the same system of 1D PDEs.

More precisely, if $\widetilde{X}$ designates — for any fluid quantity X — the corresponding perturbation modal component of spherical harmonics degree l, the system of 1D PDEs to be solved for consists in:

(i) an inhomogeneous system of 1D linear conservation laws for the vector of conservative variable perturbation modal components $\widetilde{\mathbf{U}}$, or

$$\partial_t\widetilde{\mathbf{U}} + \partial_m\Big[A\,\widetilde{\mathbf{F}}\big(\mathbf{U},\widetilde{\mathbf{U}}\big)\Big] + \tau\,\widetilde{\mathbf{F}}^{\perp}\big(\mathbf{U},\widetilde{\Omega}\big) + \partial_m\Big[\widetilde{A}\,\mathbf{F}(\mathbf{U})\Big] + \partial_m\big[A\,\mathbf{F}(\mathbf{U})\big]\,\widetilde{\Theta} = \widetilde{\mathbf{G}}\big(\mathbf{U},\widetilde{\mathbf{U}}\big) + \mathbf{G}(\mathbf{U})\,\widetilde{\Theta}, \quad (2)$$

with the conventions of Eq. (1) and the definitions

$$\begin{gathered}\widetilde{A} = 2r\widetilde{r}, \quad \widetilde{\mathbf{U}} = \big(\widetilde{\tau},\ \widetilde{u},\ \widetilde{e}\big)^{\top}, \quad \widetilde{\mathbf{F}}\big(\mathbf{U},\widetilde{\mathbf{U}}\big) \equiv \frac{d\mathbf{F}}{d\mathbf{U}}(\mathbf{U})\,\widetilde{\mathbf{U}} = \big(-\widetilde{u},\ \widetilde{p},\ p\,\widetilde{u} + \widetilde{p}\,u\big)^{\top}, \\ \widetilde{\mathbf{F}}^{\perp}\big(\mathbf{U},\widetilde{\Omega}\big) = \big(-\widetilde{\Omega},\ 0,\ p\,\widetilde{\Omega}\big)^{\top}, \quad \widetilde{\mathbf{G}}\big(\mathbf{U},\widetilde{\mathbf{U}}\big) = \big(0,\ p\,\partial_m\widetilde{A} + \widetilde{p}\,\partial_m A,\ 0\big)^{\top},\end{gathered} \quad (3)$$

(ii) time-differential equations for the modal components, $\widetilde{r}$ and $\widetilde{\Theta}$, of the Lagrangian radial displacement and transverse motion dilatation perturbations, namely

$$\partial_t\big(A\,\widetilde{\Omega}\big) = -\mathrm{w}\,\big(\tau\,\widetilde{p} + p\,\partial_m\big[A\,\widetilde{r}\big] - \partial_m\big[A\,\widetilde{r}\,p\big]\big)\,, \quad \text{with } \mathrm{w} = -l(l+1), \quad (4a)$$

$$\partial_t\widetilde{r} = \widetilde{u}, \quad (4b)$$

$$\partial_t\widetilde{\Theta} = \widetilde{\Omega}, \quad (4c)$$

(iii) a modal component form of the mass conservation equation perturbation, here

$$\widetilde{\tau} = \partial_m\big(A\,\widetilde{r}\big) + \tau\,\widetilde{\Theta}. \quad (5)$$

This set of equations is supplemented by the fluid linearized equations of state under the form

$$\widetilde{p} = P_{\tau}\big(\tau,\mathcal{E}\big)\,\widetilde{\tau} + P_{\mathcal{E}}\big(\tau,\mathcal{E}\big)\,\widetilde{\mathcal{E}}, \quad (6)$$

with $\widetilde{\mathcal{E}} = \widetilde{e} - u\,\widetilde{u}$, and where P_τ and $P_\mathcal{E}$ stand for the thermodynamical partial derivatives $(\partial P/\partial\tau)_\mathcal{E}$ and $(\partial P/\partial\mathcal{E})_\tau$, respectively.

The above formulation (2)–(4) of the perturbation modal component equations — borrowed from [5, Sec. 1.3] — is in fact generic to both planar and spherical symmetries, the equations in the former case being recovered upon considering that $A = 1$, and therefore $\widetilde{A} = 0$, along with the appropriate definitions of the transverse motion dilatation $\widetilde{\Theta}$, expansion $\widetilde{\Omega}$, and of the coefficient w [13, Sec. 2.2.2 and Eq. (B.7)]. Hence in both cases the 1D conservation law system (2) involves the linearization of the basic flow 1D flux function, $\frac{d\mathbf{F}}{d\mathbf{U}}(\mathbf{U})\,\widetilde{\mathbf{U}}$, which acts as the flux function *along the longitudinal direction* for the conservative variable modal components $\widetilde{\mathbf{U}}$, the flux function relevant to *the transverse direction* intervening in the contribution $\widetilde{\mathbf{F}}^\perp\big(\mathbf{U},\widetilde{\Omega}\big)$. A comparison between the two respective systems indicates that the additional terms induced by the spherical geometry are not necessarily issuing from a mere linearization of the terms present in the basic flow system (1): cf. the term $\mathbf{G}(\mathbf{U})\,\widetilde{\Theta}$ on the right-hand-side of (2).

In fact, a better understanding of the different terms involved in (2) may be gained from considering the finite-volume formulation of this system, that is

$$\partial_t\widetilde{\mathbf{U}} + \partial_m\Big[A\,\widetilde{\mathbf{F}}\big(\mathbf{U},\widetilde{\mathbf{U}}\big)\Big] + \tau\,\widetilde{\mathbf{F}}^\perp\big(\mathbf{U},\widetilde{\Omega}\big) + \partial_m\Big[\big(\widetilde{A} + A\,\widetilde{\Theta}\big)\,\mathbf{F}(\mathbf{U})\Big] = \begin{pmatrix} -u\,A\,\partial_m\widetilde{\Theta} \\ p\,\partial_m\big[\widetilde{A} + A\,\widetilde{\Theta}\big] + \widetilde{p}\,\partial_m A \\ p\,u\,A\,\partial_m\widetilde{\Theta} \end{pmatrix}. \tag{7}$$

Although this very formulation will not be used when devising the linear perturbation modal component numerical scheme, its analysis will provide useful guidelines when discretizing the different terms of Eq. (2). Such an analysis is summarized in Table 1 by listing the different contributions which are involved in Eqs. (4a) and (7), in connection with the actions of the geometrical deformation field $(\widetilde{r},\widetilde{\Theta})$ and of the fluid motion perturbation. Whence it appears that the different terms of Eqs. (2) and (4a) which involve the geometrical quantities $\widetilde{A}$, $\widetilde{\Theta}$ and $A\,\widetilde{r}$, should be viewed as deriving from a formulation of the fluid motion equations on a moving deformed grid. This last point has important implications in terms of discretization and constitutes the essential difficulty in devising a proper numerical scheme for the system of equations (2)–(4). Indeed, the problem raised by the fact that system (2) — as its planar-symmetric 1D basic-flow counterpart [13, Eq. (18a)] — is a first-order linear system with possibly discontinuous coefficients, has already been considered in the simpler setting of planar geometry: cf. [22, 13]. Therefore, the linearized numerical fluxes which have then been proposed and shown to yield adequate results [22, 13], may be directly used in the present case.

3. NUMERICAL SCHEME

In this section, we present a two-level explicit numerical scheme for solving simultaneously the nonlinear system (1) for the basic flow and the linear system (2)–(4) for the linear Lagrangian perturbation modal components.

This choice of a purely explicit scheme is justified by the following fact. An appropriate description of unsteady flows involving acoustic phenomena requires temporal samplings higher than acoustic frequencies. For a given linear perturbation modal component of degree l, such frequencies scale as l when $l \gg 1$, i. e. as would scale the inverse of the time step imposed by the stability condition of an explicit scheme for Eqs. (2)–(4) (*e. g.* see [8, 6]). Consequently, there is little or no advantage in using, at large l, an implicit rather than an explicit scheme for the modal component system (2)–(4): cf. [6].

Following the method of lines approach, the present two-level scheme must be thought as an elementary block to be used within some high-order explicit single-step multi-level time-integrating procedure. More specifically, this scheme draws from the method originally proposed by the author [11] for the case of spherically-symmetric basic flows and which relied on a linearization [39, 23, 22] of the Roe method in Lagrangian coordinates (*e. g.* see [19]), and from the

origin	equation	control surface(s)			
			$m = \mathrm{cst}$		$\mathrm{d\!l}^0\theta = \mathrm{cst}$ and $\mathrm{d\!l}^0\varphi = \mathrm{cst}$
geometrical deformations:					
• radial	(7)	$*$	$\partial_m\big[\widetilde{A}\,\mathbf{F}\big]$	$*$	$p\,\partial_m\widetilde{A}$
	(4a)	$\dagger$	$\partial_m\big[A\,\widetilde{r}\,p\big]$	$\dagger$	$p\,\partial_m\big[A\,\widetilde{r}\big]$
• transverse	(7)	$*$	$\partial_m\big[A\,\widetilde{\Theta}\,\mathbf{F}\big]$	$\dagger$	$-u\,A\,\partial_m\widetilde{\Theta},\ p\,\partial_m\big[A\,\widetilde{\Theta}\big],\ p\,u\,A\,\partial_m\widetilde{\Theta}$
motion perturbations:					
• radial	(7)		$\partial_m\big[A\,\widetilde{\mathbf{F}}\big]$		$\widetilde{p}\,\partial_m A$
• transverse	(7)		—		$\tau\,\widetilde{\mathbf{F}}^{\perp}$
	(4a)		—		$\tau\,\widetilde{p}$

TABLE 1

Relation between the different terms in Eqs. (4a) and (7) and their origin in terms of actions of the geometrical deformation field and of the fluid motion perturbation, with respect to the control surfaces of a Lagrangian elementary fluid volume defined in terms of the Lagrangian coordinate system $(m, \mathrm{d\!l}^0\theta, \mathrm{d\!l}^0\varphi)$. (See Appendix A.3.1 for more details on the notations and on this particular coordinate system.) The terms related to the deformation field are distinguished based on whether they correspond to modifications of the control surface areas ($*$) or of their inclinations ($\dagger$).

Godunov-type method, in its method-of-lines variant, which was detailed in [13, Sec. 3] for handling linear perturbations of multi-material one-dimensional flows with planar symmetry. Hence, we take from the former the mass-conservation compliant discretization [11, App. D] of the linear perturbation modal component equations but with further refinements (see Appendix C), thus inducing modifications of the corresponding scheme [13, Sec. 3.2] in planar symmetry (cf. Remark 3). From the latter, we adopt the same MUSCL-type variable reconstructions [13, Sec. 3.3.2] and the same numerical fluxes — i. e. those of a HLLC solver (*e. g.* see [47, 16, 19]) in its single acoustic impedance formulation for the basic conservative variables $\mathbf{U}$, and of its linearization [30, 13] for the conservative variable modal components $\widetilde{\mathbf{U}}$. However, we propose an alternate construction for the linearized flux by showing its equivalence with a *linearized simple Riemann solver* — i. e. a particular linearization of the simple (in the sense of Gallice [19]) Riemann solver associated to the numerical flux for the basic flow: see Appendix B. Furthermore this linearized simple Riemann solver is proved (Appendix B) to yield a Godunov-type scheme for the linearized conservative system for $\widetilde{\mathbf{U}}$, i. e. Eq. (4) where $A = 1$, $\widetilde{A} = 0$, $\mathrm{w} = 0$. Last, but not least, a numerical stability analysis of the linear perturbation scheme is provided in planar symmetry and for a uniform and constant basic flow: see Appendix D. This analysis leads to a practical time-step criterion for third-order non-degenerate Runge–Kutta time integrators, including that previously used in [13]. This criterion turns out to be sufficient in practice for ensuring the scheme numerical stability.

For the sake of the presentation, we assume that the material system under study is divided into concentric spherical shells — “cells” — $(m_{j-1/2}, m_{j+1/2})$, $j \geq 1$, of masses per steradian Δm_j which are not necessarily identical. We also consider, for $t \geq 0$, an increasing sequence (t_n), for $n \geq 0$, with

$$t_0 = 0, \quad t_{n+1} = t_n + \Delta t_n, \quad \Delta t_n > 0.$$

For any function $X(m, t)$, representing either a basic flow or a modal component quantity, we denote by $X_j(t)$ its average value over the cell $(m_{j-1/2}, m_{j+1/2})$, namely

$$X_j(t) = \frac{1}{\Delta m_j} \int_{m_{j-1/2}}^{m_{j+1/2}} X(m,t)\, dm, \quad t \geq 0,$$

and by $X_{j+1/2}(t)$ its point value $X(m_{j+1/2}, t)$. Furthermore, we convene to use the notation X^n (respectively $X^{n+1/2}$) to designate an approximation of $X(t)$ at time $t = t_n$ (respectively, for t over the interval (t_n, t_{n+1})). In addition we will use throughout this section the shorthand notations

$$\big[X\big]_{j-1/2}^{j+1/2} = X_{j+1/2} - X_{j-1/2} \quad \text{and} \quad \big[X\big]_{n}^{n+1} = X^{n+1} - X^{n}.$$

With the above conventions, the two-level explicit Godunov-type scheme that we propose for computing solutions of the nonlinear system (1) for the basic flow, and of the linear system (4) for the linear perturbation modal components, comes as, respectively,

$$\mathbf{U}_j^{n+1} = \mathbf{U}_j^{n} - \frac{\Delta t_n}{\Delta m_j} \Big[A^{n+1/2}\, \mathbf{F}(\mathbf{U})^n\Big]_{j-1/2}^{j+1/2} + \Delta t_n\, \mathbf{G}(\mathbf{U})_j^{n+1/2}, \tag{8a}$$

$$r_{j+1/2}^{n+1} = r_{j+1/2}^{n} + \Delta t_n\, {u^*}_{j+1/2}^{n}, \tag{8b}$$

and

$$\begin{aligned}
\widetilde{\mathbf{U}}_j^{n+1} = \widetilde{\mathbf{U}}_j^{n} &- \frac{\Delta t_n}{\Delta m_j} \Big[A^{n+1/2}\, \widetilde{\mathbf{F}}\big(\mathbf{U}, \widetilde{\mathbf{U}}\big)^n\Big]_{j-1/2}^{j+1/2} - \Delta t_n \big(\tau\, \widetilde{\mathbf{F}}^{\perp}\big(\mathbf{U}, \widetilde{\Omega}\big)\big)_j^{n+1/2} \\
&- \frac{\Delta t_n}{\Delta m_j} \Big[\widetilde{A}^{n+1/2}\, \mathbf{F}(\mathbf{U})^n\Big]_{j-1/2}^{j+1/2} - \frac{\Delta t_n}{\Delta m_j} \Big[A^{n+1/2}\, \mathbf{F}(\mathbf{U})^n\Big]_{j-1/2}^{j+1/2} \widetilde{\Theta}_j^{n+1/2} \\
&+ \Delta t_n \Big(\widetilde{\mathbf{G}}\big(\mathbf{U}, \widetilde{\mathbf{U}}\big)_j^{n+1/2} + \big(\mathbf{G}(\mathbf{U})\, \widetilde{\Theta}\big)_j^{n+1/2}\Big),
\end{aligned} \tag{9a}$$

$$\begin{aligned}
\big(A\, \widetilde{\Omega}\big)_j^{n+1} = \big(A\, \widetilde{\Omega}\big)_j^{n} - \Delta t_n\, \mathrm{w} \Bigg\{ \big(\tau\, \widetilde{p}\big)_j^{n+1/2} &+ \frac{p_j^{n+1/2}}{\Delta m_j} \Big[\big(A\, \widetilde{r}\big)^{n+1/2}\Big]_{j-1/2}^{j+1/2} \\
&- \frac{1}{\Delta m_j} \Big[\big(A\, \widetilde{r}\big)^{n+1/2}\, {p^*}^{n}\Big]_{j-1/2}^{j+1/2} \Bigg\},
\end{aligned} \tag{9b}$$

$$\widetilde{\Omega}_j^{n+1} = \big(A\, \widetilde{\Omega}\big)_j^{n+1} / A_j^{n+1}, \quad A_j^{n+1} = (r_j^{n+1})^2 = \big\{\big[(r_{j-1/2}^{n+1})^3 + (r_{j+1/2}^{n+1})^3\big]/2\big\}^{2/3}, \tag{9c}$$

$$\widetilde{r}_{j+1/2}^{n+1} = \widetilde{r}_{j+1/2}^{n} + \Delta t_n\, {\widetilde{u}^*}{}_{j+1/2}^{n}, \tag{9d}$$

$$\widetilde{\Theta}_i^{n+1} = \widetilde{\Theta}_i^{n} + \Delta t_n\, \widetilde{\Omega}_i^{n}, \tag{9e}$$

with the various definitions given below.

Intercell numerical fluxes As in the case of planar-symmetric basic flows [13], the intercell numerical fluxes $\mathbf{F}(\mathbf{U})_{j\pm1/2}^{n}$ in Eqs. (8a), (9a), and $\widetilde{\mathbf{F}}(\mathbf{U}, \widetilde{\mathbf{U}})_{j\pm1/2}^{n}$ in (9a) are defined, respectively, by

$$\begin{aligned}
\mathbf{F}(\mathbf{U})_{j+1/2}^{n} &= \mathbf{f}\big(\mathbf{U}_{\mathsf{L}} = \mathbf{U}_{j,+}^{n}, \mathbf{U}_{\mathsf{R}} = \mathbf{U}_{j+1,-}^{n}\big) \\
&= \Big(-{u^*}_{j+1/2}^{n},\ {p^*}_{j+1/2}^{n},\ {p^*}_{j+1/2}^{n}\, {u^*}_{j+1/2}^{n}\Big)^{\top},
\end{aligned} \tag{10}$$

$$\begin{aligned}
\mathbf{F}\big(\mathbf{U}, \widetilde{\mathbf{U}}\big)_{j+1/2}^{n} &= \widetilde{\mathbf{f}}\big(\mathbf{U}_{\mathsf{L}} = \mathbf{U}_{j,+}^{n}, \mathbf{U}_{\mathsf{R}} = \mathbf{U}_{j+1,-}^{n}, \widetilde{\mathbf{U}}_{\mathsf{L}} = \widetilde{\mathbf{U}}_{j,+}^{n}, \widetilde{\mathbf{U}}_{\mathsf{R}} = \widetilde{\mathbf{U}}_{j+1,-}^{n}\big) \\
&= \Big(-{\widetilde{u}^*}{}_{j+1/2}^{n},\ {\widetilde{p}^*}{}_{j+1/2}^{n},\ {p^*}_{j+1/2}^{n}\, {\widetilde{u}^*}{}_{j+1/2}^{n} + {\widetilde{p}^*}{}_{j+1/2}^{n}\, {u^*}_{j+1/2}^{n}\Big)^{\top},
\end{aligned} \tag{11}$$

with the expressions

$$\mathbf{f}\big(\mathbf{U}_\mathsf{L},\mathbf{U}_\mathsf{R}\big) = (-u^*,\ p^*,\ p^*\,u^*)^\top, \qquad \begin{cases} u^* = (\Sigma u - \Delta p/C^*)\,/2, \\ p^* = (\Sigma p - C^*\,\Delta u)\,/2, \end{cases} \tag{12}$$

$$\widetilde{\mathbf{f}}\big(\mathbf{U}_\mathsf{L},\mathbf{U}_\mathsf{R},\widetilde{\mathbf{U}}_\mathsf{L},\widetilde{\mathbf{U}}_\mathsf{R}\big) = (-\widetilde{u}^*,\ \widetilde{p}^*,\ p^*\,\widetilde{u}^* + \widetilde{p}^*\,u^*)^\top, \qquad \begin{cases} \widetilde{u}^* = (\Sigma\widetilde{u} - \Delta\widetilde{p}/C^*)\,/2, \\ \widetilde{p}^* = (\Sigma\widetilde{p} - C^*\,\Delta\widetilde{u})\,/2, \end{cases} \tag{13}$$

with the convention $\Sigma X = X_\mathsf{L} + X_\mathsf{R}$ and $\Delta X = X_\mathsf{R} - X_\mathsf{L}$. The notations $\mathbf{U}^n_{j,\pm}$ ($\widetilde{\mathbf{U}}^n_{j,\pm}$) designate some extrapolated values, at the cell edges $m_{j\pm1/2}$, of the cell-averaged state $\mathbf{U}^n_j$ (respectively $\widetilde{\mathbf{U}}^n_j$). Piecewise constant extrapolations lead to a spatially first-order accurate scheme, while higher-order space approximations is achieved *via* a MUSCL reconstruction (*e. g.* see [47]). In effect we use the same MUSCL-type reconstruction methods as those previously tested for planar-symmetric basic flows (see [13, Sec. 3.3.2]): one consisting in a variant of the so-called "slope-limiting in local characteristic variables", the other relying on an extrapolation in the primitive variables $(\tau, u, \mathcal{E})$. As in [13], the parameter C^* of the formulas (12) and (13) is chosen to be [15, Ann. D]

$$C^* = \sqrt{\max\left\{\tau_\mathsf{L}\,C_\mathsf{L}^2, \tau_\mathsf{R}\,C_\mathsf{R}^2\right\}/\max\left\{\tau_\mathsf{L},\tau_\mathsf{R}\right\}}\,, \tag{14}$$

where C denotes the acoustic impedance — or Lagrangian speed of sound — related to a given state $\mathbf{U}$, i. e.

$$C = \sqrt{p\,P_\mathcal{E} - P_\tau}.$$

Other choices for C^* are possible as discussed, for example, in [16, 19].

The expression (13) of the numerical flux $\widetilde{\mathbf{f}}(\mathbf{U}_\mathsf{L},\mathbf{U}_\mathsf{R},\widetilde{\mathbf{U}}_\mathsf{L},\widetilde{\mathbf{U}}_\mathsf{R})$ was initially introduced in [30, 13] as a linearization of the flux $\mathbf{f}\big(\mathbf{U}_\mathsf{L},\mathbf{U}_\mathsf{R}\big)$, by exploiting the canonical formulation of the 1D gas dynamics Lagrangian equations by Després [16]. It has been shown by Gallice [19, Propos. 5] that the numerical flux $\mathbf{f}\big(\mathbf{U}_\mathsf{L},\mathbf{U}_\mathsf{R}\big)$ of (12) is in fact associated to the *simple Riemann solver*

$$\mathbf{W}(\mu/t;\mathbf{U}_\mathsf{L},\mathbf{U}_\mathsf{R}) = \begin{cases} \mathbf{U}_1 = \mathbf{U}_\mathsf{L}, & \mu/t < -C^*, \\ \mathbf{U}_2 = \mathbf{U}_\mathsf{L} + \alpha_1\,\mathbf{R}_1, & -C^* < \mu/t < 0, \\ \mathbf{U}_3 = \mathbf{U}_\mathsf{R} - \alpha_3\,\mathbf{R}_3, & 0 < \mu/t < C^*, \\ \mathbf{U}_4 = \mathbf{U}_\mathsf{R}, & C^* < \mu/t, \end{cases} \tag{15}$$

where μ is the Lagrangian mass variable in planar symmetry (i. e. $d\mu = \rho\,dx$), and where

$$\begin{gathered} \mathbf{R}_1 = \big(-1,\ -C^*,\ (\Sigma p - C^*\,\Sigma u)/2\big)^\top, \quad \mathbf{R}_3 = (-1,\ C^*,\ (\Sigma p + C^*\,\Sigma u)/2)^\top, \\ \alpha_1 = (\Delta p - C^*\Delta u)\,/2\,{C^*}^2, \quad \alpha_3 = (\Delta p + C^*\Delta u)\,/2\,{C^*}^2, \end{gathered} \tag{16}$$

are the right eigenvectors and characteristic variables associated to the $-C^*$ and $+C^*$ eigenvalues of a Roe-type matrix for the states $(\mathbf{U}_\mathsf{L},\mathbf{U}_\mathsf{R})$. The converse is true for the linearized numerical flux $\widetilde{\mathbf{f}}(\mathbf{U}_\mathsf{L},\mathbf{U}_\mathsf{R},\widetilde{\mathbf{U}}_\mathsf{L},\widetilde{\mathbf{U}}_\mathsf{R})$: the expression (13) is nothing else but that of the numerical flux associated to the *linearized simple Riemann solver*

$$\widetilde{\mathbf{W}}(\mu/t;\mathbf{U}_\mathsf{L},\mathbf{U}_\mathsf{R},\widetilde{\mathbf{U}}_\mathsf{L},\widetilde{\mathbf{U}}_\mathsf{R}) = \begin{cases} \widetilde{\mathbf{U}}_1 = \widetilde{\mathbf{U}}_\mathsf{L}, & \mu/t < -C^*, \\ \widetilde{\mathbf{U}}_2 = \widetilde{\mathbf{U}}_\mathsf{L} + \widetilde{\alpha}_1\,\mathbf{R}_1 + \alpha_1\,\widetilde{\mathbf{R}}_1, & -C^* < \mu/t < 0, \\ \widetilde{\mathbf{U}}_3 = \widetilde{\mathbf{U}}_\mathsf{R} - \widetilde{\alpha}_3\,\mathbf{R}_3 - \alpha_3\,\widetilde{\mathbf{R}}_3, & 0 < \mu/t < C^*, \\ \widetilde{\mathbf{U}}_4 = \widetilde{\mathbf{U}}_\mathsf{R}, & C^* < \mu/t, \end{cases} \tag{17}$$

where

$$\begin{gathered} \widetilde{\mathbf{R}}_1 = (0,\ 0,\ (\Sigma\widetilde{p} - C^*\,\Sigma\widetilde{u})/2)^\top, \quad \widetilde{\mathbf{R}}_3 = (0,\ 0,\ (\Sigma\widetilde{p} + C^*\,\Sigma\widetilde{u})/2)^\top, \\ \widetilde{\alpha}_1 = (\Delta\widetilde{p} - C^*\Delta\widetilde{u})\,/2\,{C^*}^2, \quad \widetilde{\alpha}_3 = (\Delta\widetilde{p} + C^*\Delta\widetilde{u})\,/2\,{C^*}^2, \end{gathered} \tag{18}$$

see Appendix B. This result establishes the equivalence between the numerical flux (13) and the simple Riemann solver (17), (18) obtained as a "natural" linearization of the solver (15), (16). We thus have a full characterization of the resulting scheme in terms of linear perturbations of the basic-flow solver elementary waves.

Flux contributions and geometric conservation law considerations In view of the discussion of Section 2, the contributions of the intercell numerical fluxes $\mathbf{F}(\mathbf{U})^n_{j+1/2}$ and $\widetilde{\mathbf{F}}(\mathbf{U},\widetilde{\mathbf{U}})^n_{j+1/2}$ to Eqs. (8a) and (9a) should involve approximations of the area $A_{j+1/2}$, its modal component $\widetilde{A}_{j+1/2}$, and of the modal transverse dilatation $\widetilde{\Theta}_j$ over the time interval (t_n, t_{n+1}). Given the definition (10) of $\mathbf{F}(\mathbf{U})^n_{j+1/2}$, the correct approximation $A^{n+1/2}_{j+1/2}$ of the area $A_{j+1/2}$ is obtained by requiring the scheme (8) to satisfy the discrete formulation of the mass conservation law — or, equivalently here, of the geometric conservation law [46]. This requirement yields the well-known result (*e. g.* see [45])

$$A^{n+1/2}_{j+1/2} = A^n_{j+1/2} + \Delta t_n\, {u^*}^n_{j+1/2}\Big(r^n_{j+1/2} + \Delta t_n\, {u^*}^n_{j+1/2}/3\Big), \tag{19}$$

where $A^n_{j+1/2} = (r^n_{j+1/2})^2$. The same principle evidently applies to the scheme (9) for the modal motion, leading to the definitions [11, Eq. (D.3)]

$$\widetilde{A}^{n+1/2}_{j+1/2} = \widetilde{A}^n_{j+1/2} + \Delta t_n \left[{u^*}^n_{j+1/2}\, \widetilde{r}^n_{j+1/2} + {\widetilde{u}^*}{}^n_{j+1/2}\left(r^n_{j+1/2} + 2\,\Delta t_n\, {u^*}^n_{j+1/2}/3\right)\right], \tag{20}$$

where $\widetilde{A}^n_{j+1/2} = 2\, r^n_{j+1/2}\, \widetilde{r}^n_{j+1/2}$, and

$$\widetilde{\Theta}^{n+1/2}_j = \widetilde{\Theta}^{n+1}_j, \tag{21}$$

see Appendix C. Hence, the application of the discrete geometric conservation law not only stipulates the definition of the area term $\widetilde{A}^{n+1/2}_{j+1/2}$ which is specific to spherical symmetry, but also that of the transverse dilatation approximant $\widetilde{\Theta}^{n+1/2}_j$ for both types of symmetry (cf. Appendix C, Remark 3).

Symmetry and other pressure term contributions As in [13], the basic and modal pressures applying to the lateral surfaces of a Lagrangian fluid element (see Table 1) are considered to be constant for (m,t) in $(m_{j-1/2}, m_{j+1/2}) \times (t_n, t_{n+1})$. This choice and that of favoring explicit estimates, result in the definitions:

$$\big(\tau\, \widetilde{\mathbf{F}}^{\perp}(\mathbf{U},\widetilde{\Omega})\big)^{n+1/2}_j = \tau^n_j\, \big(-\widetilde{\Omega}^n_j,\ 0,\ p^n_j\, \widetilde{\Omega}^n_j\big)^{\top}, \tag{22}$$

for the contribution to Eq. (9a) of the transverse fluxes for $\widetilde{\tau}$ and $\widetilde{e}$;

$$\mathbf{G}(\mathbf{U})^{n+1/2}_j = \Big(0,\ p^n_j\, \big[A^{n+1/2}\big]^{j+1/2}_{j-1/2}/\Delta m_j,\ 0\Big)^{\top}, \tag{23}$$

for the symmetry term in Eq. (8a);

$$\widetilde{\mathbf{G}}(\mathbf{U},\widetilde{\mathbf{U}})^{n+1/2}_j = \Big(0,\ \Big\{p^n_j\, \big[\widetilde{A}^{n+1/2}\big]^{j+1/2}_{j-1/2} + \widetilde{p}^n_j\, \big[A^{n+1/2}\big]^{j+1/2}_{j-1/2}\Big\}/\Delta m_j,\ 0\Big)^{\top}, \tag{24}$$

$$\big(\mathbf{G}(\mathbf{U})\,\widetilde{\Theta}\big)^{n+1/2}_j = \mathbf{G}(\mathbf{U})^{n+1/2}_j\, \widetilde{\Theta}^{n+1}_j, \tag{25}$$

for this symmetry term modal component contributions to Eq. (9a), the latter being defined in agreement with the definition (21); and

$$\big(\tau\, \widetilde{p}\big)^{n+1/2}_j = \tau^n_j\, \widetilde{p}^n_j, \quad p^{n+1/2}_j = p^n_j, \tag{26}$$

in the discrete modal transverse motion expansion equation (9b). In these formulas, the pressure constants are taken to be

$$p^n_j = P\big(\tau^n_j, \mathcal{E}^n_j\big), \quad \widetilde{p}^n_j = P_\tau\big(\tau^n_j, \mathcal{E}^n_j\big)\, \widetilde{\tau}^n_j + P_{\mathcal{E}}\big(\tau^n_j, \mathcal{E}^n_j\big)\, \widetilde{\mathcal{E}}^n_j,$$

with $\mathcal{E}_j^n = e_j^n - (u_j^n)^2/2$ and $\widetilde{\mathcal{E}}_j^n = \widetilde{e}_j^n - u_j^n\,\widetilde{u}_j^n$, while the approximants $A_{j+1/2}^{n+1/2}$ and $\widetilde{A}_{j+1/2}^{n+1/2}$ arise as the exact expressions of the time-averaged values of $A_{j+1/2}$ and $\widetilde{A}_{j+1/2}$, given the linear interpolations

$$r_{j+1/2}(t) = r_{j+1/2}^n + (t - t_n)\, {u^*}_{j+1/2}^n, \quad \text{and} \quad \widetilde{r}_{j+1/2}(t) = \widetilde{r}_{j+1/2}^n + (t - t_n)\, {\widetilde{u}^*}{}_{j+1/2}^n,$$

for $t_n \le t \le t_{n+1}$. Similarly, the definition

$$\left(A\,\widetilde{r}\right)_{j+1/2}^{n+1/2} = A_{j+1/2}^{n+1/2}\,\widetilde{r}_j^n + \Delta t_n\, {\widetilde{u}^*}{}_{j+1/2}^n \left[\frac{1}{2}\,A_{j+1/2}^n + \Delta t_n\, {u^*}_{j+1/2}^n \Big(\frac{2}{3}\, r_{j+1/2}^n + \frac{\Delta t_n}{4}\, {u^*}_{j+1/2}^n\Big)\right], \tag{27}$$

in Eq. (9b), proceeds from the time-averaged value of the product $A_{j+1/2}\,\widetilde{r}_{j+1/2}$.

One may check that the above definitions (23)–(27) comply with the necessary requirement of maintaining any equilibrium state with uniform pressure whatever the geometrical deformation field $(\widetilde{r}, \widetilde{\Theta})$ may be.

Time integration scheme and time-step constraints As pointed out by a numerical stability analysis (see Appendix D), the two-level explicit scheme (9) requires time integrators capable of handling purely imaginary eigenvalues. This requirement is here fulfilled by using the third-order Runge–Kutta scheme [43] previoulsy employed in [13], but here in conjunction with a specific stability condition for the modal component scheme. Consequently the computation time step is subject to the following three constraints:

- *Monotonicity of the sequence* $(r_{j+1/2}^n)$ Independently of any numerical stability condition, the time step Δt_n must be such that the monotonicity, with respect to the index j, of the sequence $(r_{j+1/2}^n)$, which satisfies the recursion (9d), is preserved whatever $n > 0$, whence the time-step constraint

$$\Delta t_n \max_j \Big\{ - \big[u^{*n}\big]_{j-1/2}^{j+1/2} \Big/ \big[r^n\big]_{j-1/2}^{j+1/2} \Big\} < 1. \tag{28}$$

- *Stability of the basic flow scheme* The following constraint is applied

$$\Delta t_n \max_j \big\{ \tau_j^n\, \overline{C}_j^n / \Delta r_j^n \big\} \le 1, \tag{29a}$$

  where

$$\overline{C}_j^n = \max\Big\{ \big({C^*}_{j-1/2}^n + {C^*}_{j+1/2}^n\big)/2, \big(1/{C^*}_{j-1/2}^n + 1/{C^*}_{j+1/2}^n\big)(C_j^n)^2/2 \Big\}, \tag{29b}$$

  for which the scheme (8), in planar symmetry, with the definition (14) has been shown to be entropic [15, Ann. D].

- *Stability of the flow modal component scheme* The time-step constraint for ensuring the stability of the scheme (9) is simply taken to be that established in the planar symmetry case, namely Eqs. (90)–(92), but with the formula

$$\mathfrak{N}_j^n = 2\pi\, r_j^n\, \big(\sqrt{|\mathrm{w}|}\, \Delta r_j^n\big)^{-1}, \tag{30}$$

  for the definition of the number of cells per transverse wavelength.

Remark 1. As is usual (*e. g.* see [21]), an equivalent formulation of the scheme (8) may be obtained upon replacing the forward recursion for (τ_j^n) in Eq. (8a) by the relation

$$\tau_j^{n+1} = \big[r^{n+1}\big]_{j-1/2}^{j+1/2}\, \big(A_{j-1/2}^{n+1} + r_{j-1/2}^{n+1}\, r_{j+1/2}^{n+1} + A_{j+1/2}^{n+1}\big)/(3\,\Delta m_j), \tag{31}$$

which simply expresses the mass conservation of the shell $(m_{j-1/2}, m_{j+1/2})$, while the converse formulation of (9) would replace the forward recursion for $(\widetilde{\tau}_j^n)$ by the discrete approximation of the modal mass conservation equation (5), in effect

$$\widetilde{\tau}_j^{n+1} = \frac{1}{\Delta m_j}\left[A^{n+1}\,\widetilde{r}^{n+1}\right]_{j-1/2}^{j+1/2} + \tau_j^{n+1}\,\widetilde{\Theta}_j^{n+1}. \tag{32}$$

Remark 2. The present modal component scheme (9) relies on the formulation of Eq. (2) rather than that of Eq. (7). This choice is based on practical considerations about the spatial discretization of the quantities $\widetilde{\Theta}$ and $\widetilde{\Omega}$. Indeed, a numerical approximation of Eq. (7) would have implied defining cell-edge values for the transverse dilatation $\widetilde{\Theta}$, thus raising the additional difficulty of handling accurately the discontinuities of $\widetilde{\Theta}$ and $\widetilde{\Omega}$ that may develop at intercell edges such as in perturbation shear motions. On the other hand, the form of Eq. (2) — as that of [13, Eqs. (32), (33), (35)] in planar symmetry — is suitable for a discrete representation of $\widetilde{\Theta}$ and $\widetilde{\Omega}$ by their cell-averaged values, thus accounting for any intercell discontinuity of these quantities in a simple way.

Remark 3. The definitions (21) and (27) have their equivalents in the planar symmetric case, thus inducing a modification of the corresponding scheme previously proposed in [13, Eqs. (32), (33), (35)].

4. NUMERICAL RESULTS

The numerical scheme detailed in the preceding section has been tested in two different spherical geometry configurations which have been chosen in relation with ICF pellet implosion features. These tests are complementary to the configurations of a single interface separating two different fluids which were treated in planar geometry in [13]. Indeed, the modifications implied by the planar-symmetric version of Eq. (9) are minor (cf. Remark 3) with respect to the scheme [13, Eqs. (32)–(35)], so that the multi-material flow capabilities shown in [13] are shared by the present scheme. Consequently, the configurations below involve a single fluid while focusing on the specific features of compressible converging flows in spherical symmetry.

The first configuration (Section 4.1) corresponds to the homogeneous isentropic compression of a polytropic gas and has been used in different instances in the context of ICF (*e. g.* see [32, 3, 26]) for studying Rayleigh–Taylor instabilities and testing the ability of multi-D fluid codes at rendering such phenomena. This configuration has the advantage of presenting distinctive features of ICF pellet implosions — isentropic compression, high convergence and compression ratios — while being given by an explicit exact solution. Moreover, reference solutions may be produced for incompressible irrotational deformation modes, ascribable to Rayleigh–Taylor modes, of such compression flows. The second configuration (Section 4.2) — a self-similar converging spherical shock wave — has been retained since it is at the heart of studies on the dynamics and stability of converging spherical shocks: see [9, 48, 10]. For this configuration, of broader interest than the sole scope of ICF pellet implosions, an analytic approximate, although accurate, description of the flow behind the converging shock [10] is available for reference. However no equivalent description exists for the linear perturbation evolution of the shock front, leading us to rely on the best available results [9, 8] and on a systematic convergence study, in terms of the number of cells per transverse wavelength $\mathfrak{N}$ of Eq. (30).

Having in mind practical applications to ICF pellet implosions where perturbations involve spherical harmonics of degrees up to several hundreds (*e. g.* see [25, 12]), the harmonics degree sequence l = 4, 16, 64, 256, 1024 has been retained for all the tests detailed below. Numerical results reported in the following have been obtained with the characteristic-variable MUSCL reconstruction variant of the scheme (8), (9) using a fifteen-digit floating-point representation.

4.1. Free surface perturbations of a uniformly imploding shell

The particular case of homogeneous compression [32, 3, 26] that we are considering, corresponds to a hollow shell of perfect gas ($\gamma = 5/3$) and uniform density which collapses from a state of rest over a unit of time. The unperturbed shell initial state is thus defined by the uniform density and quadratic pressure profiles [26]

$$\rho(r,0) = \rho^0, \quad \text{and} \quad p(r,0) = p^0\big|_{\Gamma_\mathrm{o}} \left\{1 + \rho^0 \left(r^0|_{\Gamma_\mathrm{o}}\right)^2 \left[\left(r/r^0|_{\Gamma_\mathrm{o}}\right)^2 - 1\right] / (2\,p^0\big|_{\Gamma_\mathrm{o}})\right\}, \tag{33}$$

for $r^0|_{\Gamma_\mathrm{i}} \leq r \leq r^0|_{\Gamma_\mathrm{o}}$, where Γ_i (Γ_o) denotes the shell inner (outer) boundary, along with initial boundary pressure conditions $p(r^0|_{\Gamma_\mathrm{i}/\Gamma_\mathrm{o}}, 0) = p^0|_{\Gamma_\mathrm{i}/\Gamma_\mathrm{o}}$. The shell adiabatic homogeneous compression [32], or "uniform implosion", which follows from applying the boundary pressures

$$p|_{\Gamma_\mathrm{i}/\Gamma_\mathrm{o}}(t) = p^0|_{\Gamma_\mathrm{i}/\Gamma_\mathrm{o}}\, f(t)^{-5}, \quad \text{where} \quad f(t) = \sqrt{1-t^2}, \tag{34}$$

is such that

$$r(t) = r^0\, f(t), \quad \rho(r,t) = \rho^0\, f(t)^{-3} \quad p(r,t) = p(r^0,0)\, f(t)^{-5}. \tag{35}$$

In practice, the shell initial state parameters are taken to be: $r^0|_{\Gamma_\mathrm{i}} = 0.9$, $r^0|_{\Gamma_\mathrm{o}} = 1.0$, $\rho^0 = 1.0$, $p^0|_{\Gamma_\mathrm{o}} = 1.0$.

4.1.1. Basic flow

Starting from rest at $t = 0$ with the stratification (33), implosion computations are carried out until the shell fluid particles have converged to a thousandth of their initial radial positions, i. e. for a convergence ratio, r/r^0, which is at least one order of magnitude smaller than those typically encountered in ICF pellet implosions. The accuracy of the results not only depends on the number of cells used to describe the shell stratification but also on the implementation of the chosen boundary conditions. Numerical errors (see Table 2) show good agreement with the exact solution throughout the implosion as well as convergence towards this solution as the spatial discretization is refined.

		$N = 125$	$N = 500$	$N = 2000$	$N = 8000$	$N = 32000$
$\lVert \mathsf{e}(r_{j+1/2}) \rVert_2$	PBC	$1.14\,10^{-4}$	$2.96\,10^{-5}$	$7.47\,10^{-6}$	$1.88\,10^{-6}$	$4.69\,10^{-7}$
	VBC	$1.56\,10^{-6}$	$5.18\,10^{-7}$	$1.45\,10^{-7}$	$6.86\,10^{-8}$	$8.02\,10^{-8}$
$\lVert \mathsf{e}(\rho_j) \rVert_2$	PBC	$2.24\,10^{-3}$	$5.64\,10^{-4}$	$1.41\,10^{-4}$	$3.54\,10^{-5}$	$2.39\,10^{-5}$
	VBC	$2.14\,10^{-4}$	$3.09\,10^{-5}$	$5.43\,10^{-6}$	$3.11\,10^{-6}$	$2.22\,10^{-5}$

TABLE 2
Uniformly imploding shell. L^2-norms of the relative errors on the basic-flow fluid particle radial positions and densities at the final convergence-ratio value $r/r^0 = 10^{-3}$, for increasing cell numbers N. Results obtained for mass-uniform discretizations of the shell with boundary conditions formulated in terms of pressure (PBC) or velocity (VBC).

4.1.2. Linear perturbation modal components

Two perturbed shell configurations have been considered for various spherical harmonics degrees, one for which the shell inner boundary is a free surface while the outer boundary is a rigid piston, the other being the reverse case (inner rigid piston and outer free surface). Linear incompressible irrotational deformation modes of the shell are, in the former case, neutrally stable and, in the latter case, unstable. These modes are independent of the details of the density, pressure or entropy profiles of the basic flow [3], and, as such, may be described upon applying potential flow theory to the uniform implosion of a homogeneous fluid shell. This property is presently used to furnish reference solutions for the free-surface radial linear perturbations, $\widetilde{r}_{\Gamma_\mathrm{i}/\Gamma_\mathrm{o}}$, obtained *via* the numerical integration of the ordinary differential equation satisfied by these perturbations, here with the help of a fifth-order backward differencing method (the so-called "Gear's stiff method").

Such incompressible modes may be recovered by means of compressible flow perturbation computations provided that perturbation initial conditions are sufficiently close to the exact solutions so as to minimize the importance of the compressible modes [3] which may develop during the shell implosion. Choosing the perturbed shell to be initially at rest, the flow modal component initial conditions reduce to the incompressible irrotational deformation of the shell corresponding to the boundary surface perturbation initial data. In compliance with the linear Lagrangian perturbation description of a geometrically perturbed contact discontinuity (see [13]), the discrete modal component initial values come as

$$\begin{gathered}\widetilde{\tau}_j^0 = 0, \quad \widetilde{\mathcal{E}}_j^0 = 0, \quad \widetilde{u}_j^0 = 0, \quad \widetilde{\Omega}_j^0 = 0, \\ \widetilde{r}_{j+1/2}^0 = a_l \,(r_{j+1/2}^0)^{l-1} + b_l \,(r_{j+1/2}^0)^{-l-2}, \quad \widetilde{\Theta}_j^0 = -\big[A^0\,\widetilde{r}^0\big]_{j-1/2}^{j+1/2}\big/(\tau_j^0\,\Delta m_j),\end{gathered} \tag{36}$$

where the definition of $(\widetilde{\Theta}_j^0)$ proceeds from Eq. (32) and that of $(\widetilde{r}_{j+1/2}^0)$ from the solenoidal irrotational displacement of the fluid particles, the constants a_l and b_l being determined by the boundary value equalities $\widetilde{r}_{1/2}^0 = \widetilde{r}^0|_{\Gamma_\mathrm{i}}$ and $\widetilde{r}_{N+1/2}^0 = \widetilde{r}^0|_{\Gamma_\mathrm{o}}$.

In practice, perturbation computations have been performed with pressure boundary conditions for the basic-flow.

Neutrally stable free-surface case The neutrally stable free-surface case is selected by imposing the modal component boundary conditions

$$\widetilde{p}|_{\Gamma_\mathrm{i}} = 0 \quad \text{and} \quad \widetilde{u}|_{\Gamma_\mathrm{o}} = 0, \quad \text{for } t \geq 0,$$

the initial state (36) being completed by the data $\widetilde{r}^0|_{\Gamma_\mathrm{i}} = 1$, $\widetilde{r}^0|_{\Gamma_\mathrm{o}} = 0$. The inner free surface being neutrally stable for all harmonics degrees, any damping or dispersion of the shell linear incompressible irrotational motion is immediately perceptible from the free-surface deformation results, making this test case particularly suitable for evaluating the scheme capabilities at describing free-surface perturbations in strongly convergent flows. Perturbation computations have thus been carried out, over the convergence-ratio range $10^{-3} \leq r/r^0 \leq 1$ and the spatial grid number of cells N increased until the final free-surface deformation amplitude lied within a few percents of the reference solution. This requirement can be achieved for $l \geq 16$ (see Figures 1b–d and 2) with mass-uniform shell discretizations at $\mathfrak{N} \approx 1750$, corresponding, for each of the values $l = 4,\ 16,\ 64,\ 256,\ 1024$, to the number of cells listed in Table 2. (Note that the same level of accuracy may be achieved with coarser spatial grids for a lower shell convergence.) Results for $l = 4$ (Figure 1a) cannot however be brought within this error margin due to the presence of a compressible shell-deformation mode which persists throughout the whole implosion, inducing noticeable oscillations of the computed results about the reference solution, and this regardless of the spatial grid coarseness.

Unstable free-surface case The unstable free-surface case presently treated corresponds to the initial data choice $\widetilde{r}^0|_{\Gamma_\mathrm{i}} = 0$, $\widetilde{r}^0|_{\Gamma_\mathrm{o}} = 1$ in Eq. (36), and the modal component boundary conditions

$$\widetilde{u}|_{\Gamma_\mathrm{i}} = 0 \quad \text{and} \quad \widetilde{p}|_{\Gamma_\mathrm{o}} = 0, \quad \text{for } t \geq 0.$$

Corresponding calculations performed with spatial grids at $\mathfrak{N} \approx 1750$, yield the free-surface deformation evolutions of Figure 3 with the relative errors listed in Table 3. Here, as in the neutrally stable free-surface case, free-surface deformation relative errors below a few percents are obtained for $l \geq 16$, demonstrating the scheme ability at rendering accurately this shell free-surface instability. The $l = 4$ results share the same characteristics as their neutrally-stable case equivalents: presence of an oscillatory stable compressible shell-deformation mode and error level resisting any further grid refinements. However, unstable compressible modes — characterized by time-increasing values of the modal density amplitudes and of the modal motion vorticity — are observed in all instances, illustrating the difficulty of reproducing incompressible irrotational shell-deformation modes by means of compressible flow computations.

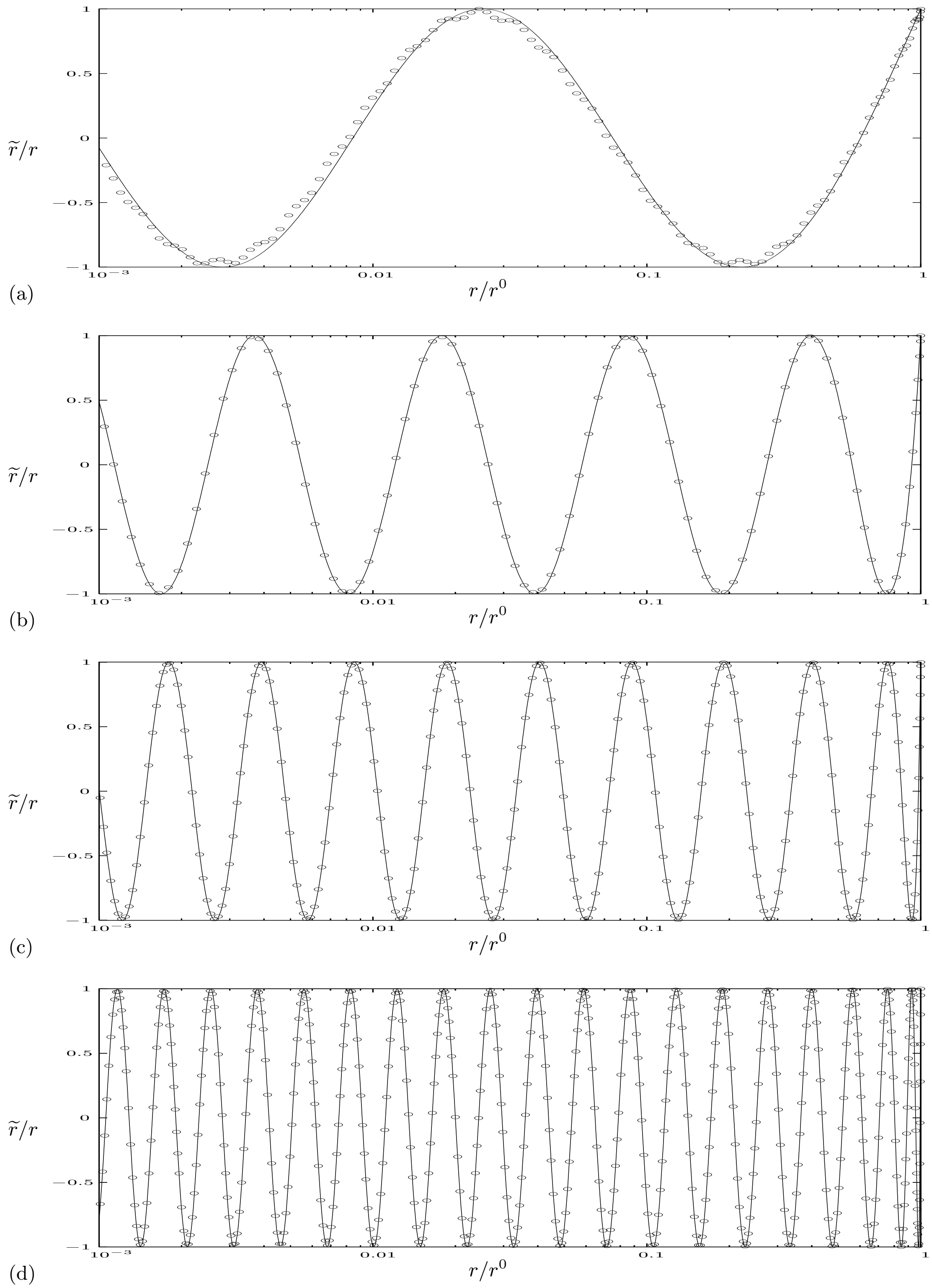

FIG. 1 Uniformly imploding shell: neutrally stable free-surface case. Comparisons of reference solutions (solid lines) and computed results (symbols) in terms of the shell inner free-surface deformation relative amplitude $\widetilde{r}/r$, plotted vs the convergence ratio r/r^0, for mode degrees: (a) $l = 4$, (b) $l = 16$, (c) $l = 64$, and (d) $l = 256$. Results obtained for mass-uniform discretizations of the shell, with, for each mode, the same minimum number of cells per transverse wavelength, $\mathfrak{N}_{\min} = 1750$.

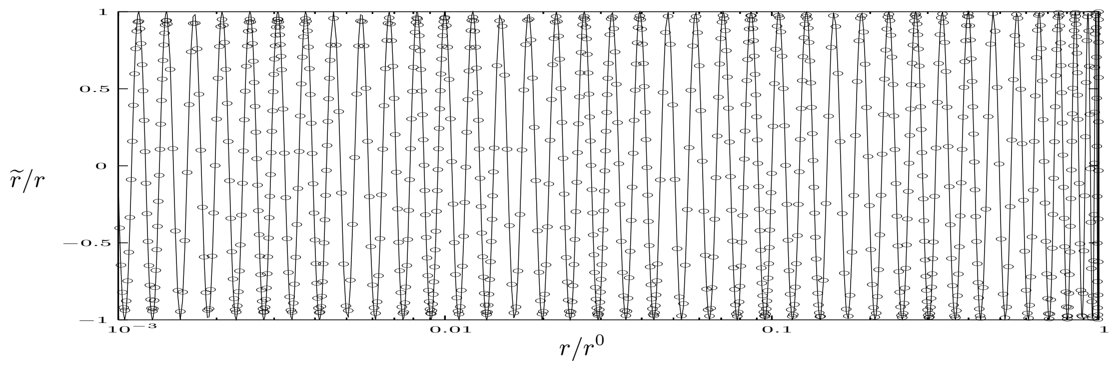

FIG. 2 Uniformly imploding shell: neutrally stable free-surface case. Comparison of reference solution (solid line) and computed result (symbols) in terms of the shell inner free-surface deformation relative amplitude $\widetilde{r}/r$, plotted vs the convergence ratio r/r^0, for mode degree $l = 1024$. Result obtained for a mass-uniform discretization of the shell corresponding to a minimum number of cells per transverse wavelength of $\mathfrak{N}_{\min} = 1750$.

	r/r^0	$l = 4$	$l = 16$	$l = 64$	$l = 256$	$l = 1024$
	10^{-1}	$4.81\,10^{-2}$	$1.24\,10^{-2}$	$6.75\,10^{-4}$	$1.52\,10^{-3}$	$1.03\,10^{-2}$
$\mathsf{e}(\widetilde{r}_{\Gamma_o})$	10^{-2}	$6.84\,10^{-2}$	$1.94\,10^{-2}$	$2.52\,10^{-4}$	$2.89\,10^{-3}$	$1.89\,10^{-2}$
	10^{-3}	$8.87\,10^{-2}$	$2.65\,10^{-2}$	$7.60\,10^{-3}$	$3.81\,10^{-3}$	$2.59\,10^{-2}$

TABLE 3

Uniformly imploding shell: unstable free-surface case. Relative errors on the shell free-surface deformation, $\mathsf{e}(\widetilde{r}_{\Gamma_o})$, at different stages of the shell convergence, for each of the mode degrees $l = 4$, 16, 64, 256, 1024. Results obtained for mass-uniform discretizations of the shell, with, for each mode, the same minimum number of cells per transverse wavelength $\mathfrak{N}_{\min} = 1750$.

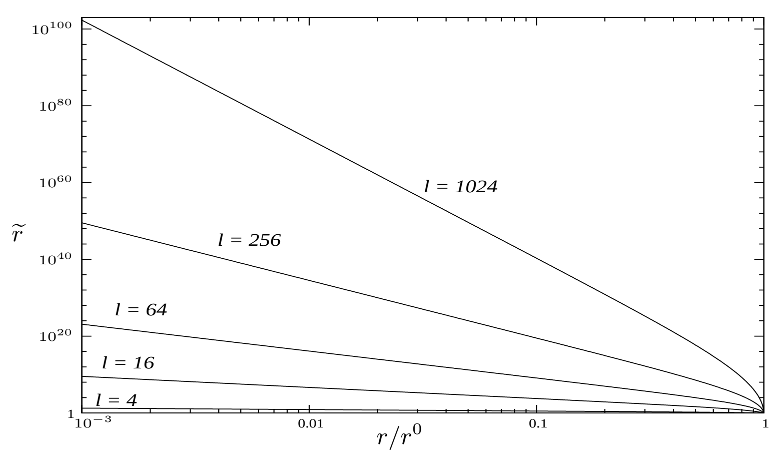

FIG. 3 Uniformly imploding shell: unstable free-surface case. Computed values of the shell outer free-surface deformation amplitude $\widetilde{r}$, plotted vs the convergence ratio r/r^0, for mode degrees: $l = 4$, 16, 64, 256, and 1024. Results obtained for mass-uniform discretizations of the shell, with, in each case, the same minimum number of cells per transverse wavelength $\mathfrak{N}_{\min} = 1750$. Computed results are graphically indistinguishable from the reference solutions (not shown). Corresponding relative errors are listed, at different stages of the shell implosion and for each mode degree, in Table 3.

From these numerical experiments, consistently achieving a given amount of error for various mode degrees l, with the MUSCL reconstruction variant of the scheme (8), (9), is seen to necessitate spatial grids with a minimum number of cells per transverse wavelength $\mathfrak{N}_{\min}$. Consequently, beyond the requirements of a given basic-flow description accuracy, the number of cells N of the grid must at least grow proportionally to l, as previously noted in [44, 8]. Inherent to this minimum $\mathfrak{N}$-value requirement is the drastic constraint that the cell size Δr must be such that

$$\Delta r \leq r/\mathfrak{N}_{\min}, \tag{37}$$

throughout the flow region. When the fluid system includes the center of symmetry, this constraint evidently needs to be relaxed as $r \to 0^+$, leading to inevitable compromises with respect to the accuracy of perturbation results in the flow central part [44]. The above inequality may also be violated during expansion flows because of the grid Lagrangian property. It must be noted that a homogeneous compression (or expansion [26]) flow of the kind of Eqs. (34), (35) constitutes a peculiar basic-flow configuration since a constant value of $\mathfrak{N}$ is automatically ensured throughout the computation by the mere fact that the spatial grid is Lagrangian. In that respect, such a configuration is inadequate at testing the stability of the flow modal component scheme (9), as illustrated by the correct homogeneous compression perturbation results obtained with the explicit first-order, whence unstable (see Appendix D), scheme of [11].

Finally, let us point out that the above spatial grid considerations equally apply to multi-D calculations with comparable numerical methods: grid numbers of cells N should scale in 2D (3D) as l^2 (respectively l^3) with cell areas (volumes) varying as r^2 (respectively r^3).

4.2. Perturbed self-similar converging shock wave

The computation of perturbed self-similar converging shock waves as presently undertaken, primarily aims at assessing the capabilities of the scheme (8), (9) at providing a quantitative description of such flows which are commonly encountered in various situations of practical interest: for example in ICF pellet implosions [20], or in the study of sonoluminescence [18]. As in the case of the perturbed homogeneous compression (Section 4.1), this series of numerical tests is profitably used to determine computational requirements that should be met in practice for obtaining meaningful descriptions of spherical shock-wave perturbations.

Since the work of Butler [9], the question of the stability of converging spherical shock waves has been the object of ongoing research: *e. g.* see [29]. Linear stability investigations — whether theoretical, with results limited to spherical harmonics of low degrees (see [9] and [8]), or numerical, using linear perturbation computation methods up to harmonics of degree $l = 100$ [24, 8] — have been carried out on the basis of self-similar converging shock-wave solutions [9, 48]. It must be noted that the most thorough numerical investigations which date back from more than twenty years ago [24, 8], still have no equivalents — whether in terms of linear perturbation computations or of multi-D simulations. The lack of multi-D fluid code results is not surprising since the accurate computation of perturbed converging shock fronts with such codes becomes rapidly overly expensive as the perturbation characteristic length is decreased. The present numerical test is the occasion of illustrating, once more, the interest and advantage of the linear computation approach by producing linear perturbation results which have no precedents in terms of accuracy and perturbation harmonics degree range.

4.2.1. Basic flow

A self-similar spherical shock-wave of infinite strength converging in an ideal gas initially at rest is characterized by a shock-front trajectory of the form [9, 48, 10]

$$r_{\mathrm{s}}(t) \propto (t_{\mathrm{c}} - t)^{\alpha}, \quad \text{for } t \leq t_{\mathrm{c}}, \tag{38}$$

where the similarity exponent α is a constant which depends on the adiabatic exponent γ, and t_{c} is the shock-front collapse time. Further description of the flow extending at infinity behind the collapsing shock wave can be found in [10]. The present test configuration is that of a ball of perfect gas ($\gamma = 5/3$), in a uniform initial state of rest, whose initial radius is taken sufficiently large ($r^0|_{\Gamma_o} = 2$) for a self-similar behavior of the computed shock fronts to be expected within the region $r_s \leq 1$. For a shock-front collapse time $t_c = 2$ and a shock-front initial radius $r_s(0) = r_s^0 = 2$, the self-similar shock-wave computation is carried out for $t \geq 0$, by applying along the ball outer boundary $r = r|_{\Gamma_o}$, the instantaneous local pressure furnished by the solution analytic description of Chisnell [10]. The validity of the self-similar solution being subject to the strong shock approximation, the gas initial state is chosen so that the initial pressure ratio across the shock is 10^6 (initial shock Mach number $M_s \approx 893$). Several spatial discretizations of the ball have been used which correspond to uniform initial values of the number of cells per transverse wavelength, $\mathfrak{N}^0$, over annular regions: cf. Table 4. The ball remaining core regions being discretized under weaker constraints, numerical results are considered as long as the computed shock fronts stay within these constant-$\mathfrak{N}^0$ annular regions. Both the computed trajectories of the shock front — here identified as the shock density-jump midpoint — and shock-wave profiles agree well with the front exact trajectory and flow analytic description [10]: see Table 4 and Figure 4. The fact that the computed shock front lags in all instances behind the exact solution, as indicated by the overestimated collapse time (Table 4), is coherent with the delayed formation of the shock wave and the associated wall-heating effects occurring early on in the computations at the outermost grid cells. Nevertheless, the favorable comparison of the numerical flow profiles taken at two different stages of the shock convergence, $r_s/r_s^0 = 0.5$ and 10^{-3}, with the solution analytic description [10] confirms the self-similar nature of the numerical solutions whence justifying their use as basic flows for investigating self-similar shock-front linear perturbations.

$\mathfrak{N}^0 = 100$	$N = 504$ $l = 4$	$N = 1970$ $l = 16$	$N = 7790$ $l = 64$	$N = 31032$ $l = 256$	$N = 86426^*$ $l = 1024$	exact
α	0.**688**6	0.**6884**4	0.**6884**3	0.**6884**2	0.**6884**5	0.68838
t_c	**2.0**1005	**2.00**441	**2.00**334	**2.00**308	**2.00**302	2

TABLE 4
Perturbed self-similar converging shock wave. Computed similarity exponents α and shock collapse times t_c. Values established by a least-square fit of Eq. (38) with the computed shock-front trajectories. Results obtained for successively refined spatial grids corresponding to uniform initial values of the number of points per transverse wavelength — namely $\mathfrak{N}^0 = 100$ — for mode degrees $l = 4$, 16, 64, 256 and 1024, over the regions $10^{-3} \leq r^0 \leq 2$ (default) or $10^{-2} \leq r^0 \leq 2$ (*). For comparison, the similarity exponent exact value [10] is also given. The significant figures in agreement with the exact values are indicated in bold, showing that an agreement to four significant figures for the similarity exponent is achieved with a moderate value of N.

4.2.2. Linear perturbation modal components

As first analyzed in [9] and later confirmed in subsequent works (see [24, 8]), modal components of self-similar converging spherical shock-front linear distortions, $\widetilde{d}_s$, are such that

$$\widetilde{d}_s \propto \mathrm{Re}(r_s^\beta), \quad \text{for } r_s > 0, \tag{39}$$

where β is a complex number whose real and imaginary parts depend on the similarity exponent α and on the modal component harmonics degree l. A spherical shock front is thus found to be unstable for moderate and bounded values of l, with $0 < \mathrm{Re}\beta < 1$ for $l \geq 2$, and to be stable, i. e. $1 < \mathrm{Re}\beta$, for sufficiently large l, while oscillating more rapidly as l increases: see [9, 24, 8]. These shock-front stability features are corroborated by computations with the scheme (8), (9) for which shock wave perturbations are introduced under the form of a unit initial deformation of the ball

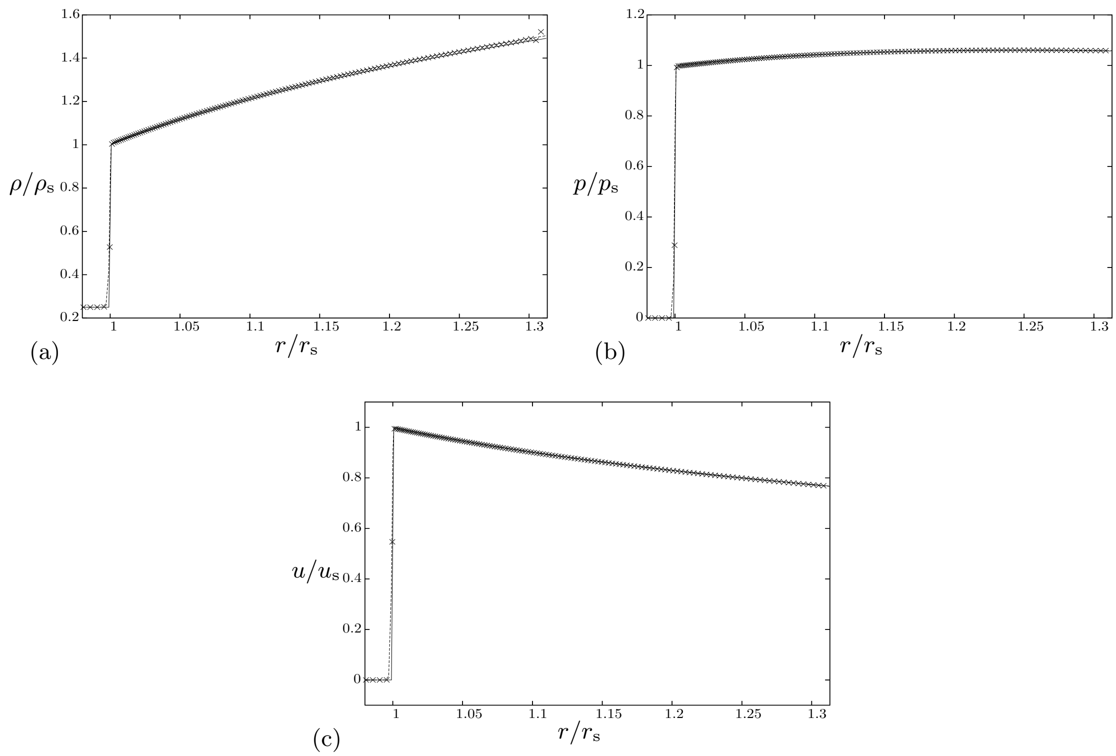

FIG. 4 Perturbed self-similar converging shock wave. Profiles of the self-similar shock wave (a) fluid density, (b) pressure and (c) fluid velocity, normalized by their value at the shock front, as function of the reduced radius r/r_{s}. Computed results obtained at two different shock-front convergence stages — $r_{\mathrm{s}}/r_{\mathrm{s}}^{0} \approx 0.5$ ($\times$) and $r_{\mathrm{s}}/r_{\mathrm{s}}^{0} \approx 10^{-3}$ (dashed line) — are compared to the corresponding analytic description (solid line) of Chisnell [10]. The discrepancies which are noticeable on the rightmost points of the fluid density profile (a) for $r_{\mathrm{s}}/r_{\mathrm{s}}^{0} \approx 0.5$ ($\times$), result from the wall-heating effect taking place at the flow outer boundary.

outer boundary surface. In effect, modal component initial values are taken to be

$$\widetilde{\tau}_j^0 = 0, \quad \widetilde{\mathcal{E}}_j^0 = 0, \quad \widetilde{u}_j^0 = 0, \quad \widetilde{\Omega}_j^0 = 0,$$
$$\widetilde{r}_{j+1/2}^0 = \delta_{jN}, \quad \widetilde{\Theta}_j^0 = -\big[A^0\, \widetilde{r}^0\big]_{j-1/2}^{j+1/2} / (\tau_j^0\, \Delta m_j),$$

δ_{jk} being Kronecker's delta symbol, in accordance with the linear Lagrangian perturbation transcription of a geometrically perturbed contact discontinuity [13]. This definition and the boundary condition $\widetilde{u}^{*n}_{N+1/2} = 0$, $n \geq 0$, make the ball outer boundary act as a corrugated piston thus launching inside the ball a deformed converging shock front for $t > 0$. The shock-front deformation $\widetilde{d}_{\mathrm{s}}$, here assimilated to the deformation of the iso-density surface given by the shock density-jump midpoint, is determined at $t = t^n$ from the discrete values, about the shock front, of the fluid density, ρ_j^n, its modal component, $\widetilde{\rho}_j^n$ and the fluid particle radial displacement, $\widetilde{r}_{j+1/2}^n$.

Shock-front deformation evolutions, obtained for increasing values of the grid parameter $\mathfrak{N}^0$ are displayed in Figures 5 and 6, and summarized in Table 5 in terms of the complex exponent β of Eq. (39). The reported values of this exponent (Table 5), established by least-square fits of Eq. (39) with appropriate subsets of the shock-front deformation records, show that, for $\mathrm{Re}\beta$, estimates which are converged within 2% (within almost 10%) are achievable with spatial grids at $\mathfrak{N}^0 = 400$ (respectively with $\mathfrak{N}^0 = 100$), while, for $\mathrm{Im}\beta$, convergence to better than 1% may be expected with grids at $\mathfrak{N}^0 = 100$. In addition Figures 5 and 6 indicate that grid $\mathfrak{N}$-parameter initial values lower than $\mathfrak{N}^0 = 100$ should be avoided and that values higher or about $\mathfrak{N}^0 = 400$ should be favored since they allow fairly accurate descriptions. The satisfactory comparison with the results of [8], obtained for mode degrees $l = 4$, 16 and 64 by means of a totally different linear perturbation scheme, contributes to the validation of the scheme (8), (9). Nevertheless, discrepancies between the different existing results for $l = 4$ (Table 5) are noticeable, pointing out the difficulty in obtaining, whether from theory or from perturbation computations, accurate descriptions of converging shock-front deformation dynamics. This difficulty is also patent from the scarceness of available data for harmonics higher than $l = 4$. In that respect the present estimates of the exponent β for $l = 256$ and 1024 constitute new contributions to the linear stability of spherical converging shock waves. However such determinations of shock-front deformation dynamics for high degree harmonics are necessarily limited due to the amount of computing they imply. For example, the calculation of the self-similar shock wave with perturbation harmonics $l = 256$ ($l = 1024$) as it converges from $r_{\mathrm{s}} = 2$ to $r_{\mathrm{s}} = 10^{-2}$ (respectively from $r_{\mathrm{s}} = 2$ to $r_{\mathrm{s}} = 10^{-1}$), on a grid with initial resolution $\mathfrak{N}^0 = 400$, amounts to over $8.24\,10^6$ (respectively $18.63\,10^6$) time-steps for $N = 86426$ (respectively $N = 195383$) cells. Given the high values of $\mathfrak{N}^0$ required for accuracy and the corresponding limited impact (see Figure 8) of the time-step constraint (90)–(92) with respect to that of the 1D basic-flow explicit scheme, computational gains offered by an implicit treatment of the perturbations such as in [31] would be limited. Rather, significant gains in computational effort could be obtained from adopting adaptive mesh refinement strategies based on the local values of the grid parameter $\mathfrak{N}$, keeping however in mind that a minimum value of $\mathfrak{N}$ should be held over some distance behind the shock front. (Indeed the description of the shock deformation depends on the rendering of downstream acoustic, entropy and vorticity modes: see Figure 7.)

The present computations of shock-wave perturbations as the shock front collapses and bounces back are inevitably subject to inaccuracies (cf. Figure 9) due to the impossibility of having a computational grid which satisifies the constraint (37) up to $r = 0$. Our experience with such perturbed shock-wave rebound calculations [12] is that these inaccuracies remain bounded and limited to the vicinity of the low $\mathfrak{N}$-parameter central region of the grid, testifying, in particular, that the time-step constraint (90)–(92) with Eq. (30) provides a sufficient condition for the modal-component scheme numerical stability. Consequently one should make sure, when devising a computational grid for a given fluid system which comprises the origin, that the low-resolution core part of the grid be of limited extent with respect to the flow regions where accurate linear perturbation data are desired. Let us emphasize that this concern is not specific to linear perturbation computations but should be taken into consideration in multi-D fluid simulations, with equivalent numerical methods, of perturbed spherically-symmetric flows.

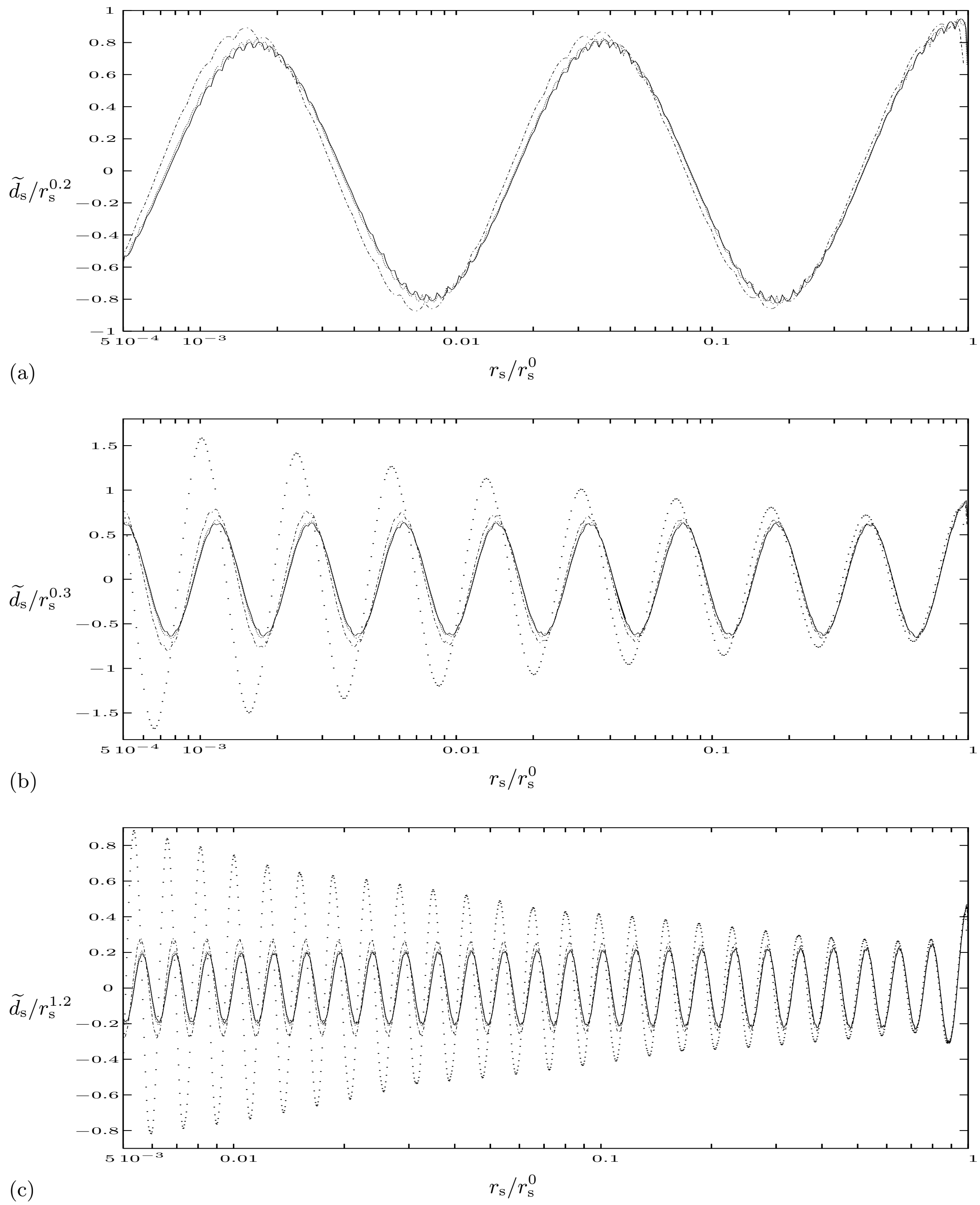

FIG. 5 Perturbed self-similar converging shock wave. Evolutions of the computed shock-front deformation $\widetilde{d}_{\rm s}$, normalized by the approximate deformation amplitude behavior (cf. Table 5), plotted vs the shock-front convergence ratio $r_{\rm s}/r_{\rm s}^{0}$ — as obtained with spatial grids of different uniform initial $\mathfrak{N}$-parameter values, $\mathfrak{N}^0 = 25$ (dots), 100 (dash-dotted line), 400 (dotted line), and 1600 (solid line) — for mode degrees: (a) $l = 4$, (b) $l = 16$, and (c) $l = 64$.

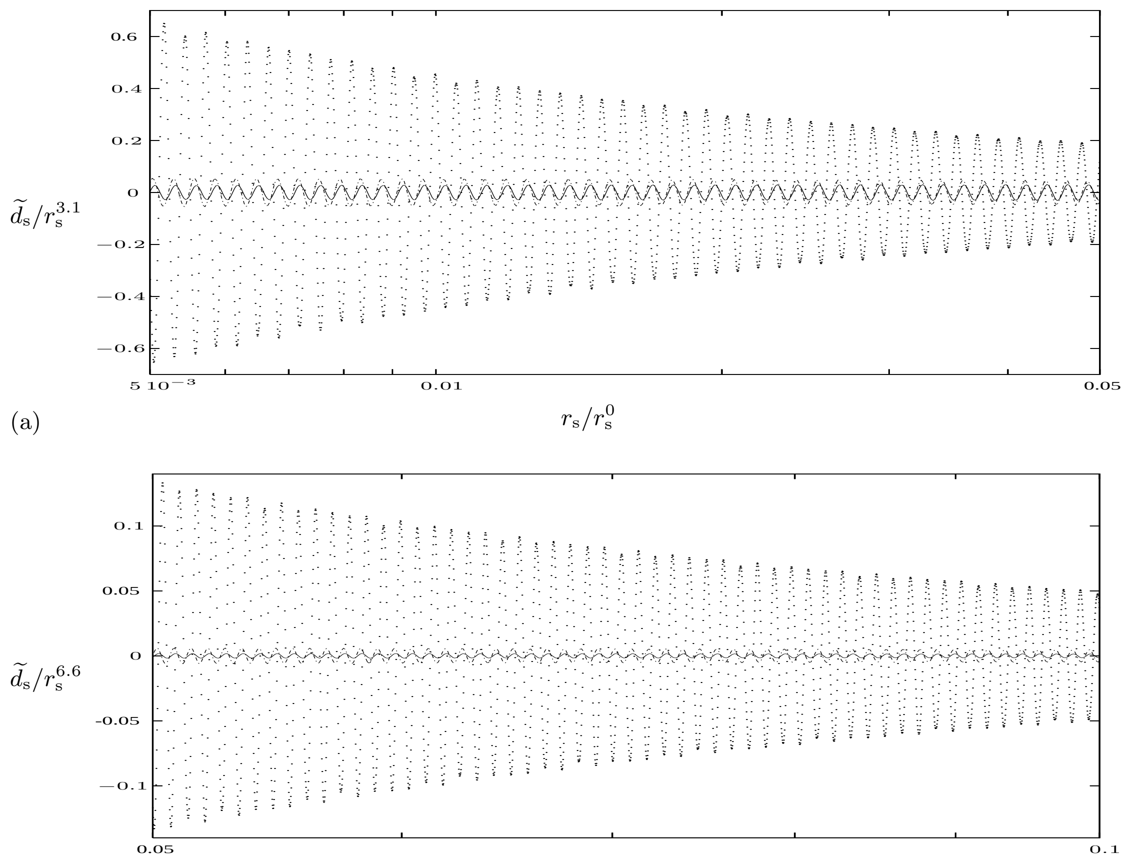

FIG. 6 Perturbed self-similar converging shock wave. Evolutions of the computed shock-front deformation $\widetilde{d}_{\mathrm{s}}$, normalized by the approximate deformation amplitude behavior (cf. Table 5), plotted vs the shock-front convergence ratio $r_{\mathrm{s}}/r_{\mathrm{s}}^{0}$ — as obtained with spatial grids of different uniform initial $\mathfrak{N}$-parameter values, $\mathfrak{N}^0 = 25$ (dots), 100 (dash-dotted line), and 400 (solid line) — for mode degrees: (a) $l = 256$ and (b) $l = 1024$.

$\mathfrak{N}^0$	$l=4$	$l=16$	$l=64$	$l=256$	$l=1024$
25	—	$0.1570 \pm \mathrm{i}\,\mathbf{7}.393$	$\mathbf{0}.9559 \pm \mathrm{i}\,\mathbf{30}.22$	$\mathbf{2}.565 \pm \mathrm{i}\,\mathbf{12}4.3$	$5.215 \pm \mathrm{i}\,\mathbf{50}4.9$
100	$0.\mathbf{1}926 \pm \mathrm{i}\,\mathbf{1.9}89$	$0.\mathbf{2}665 \pm \mathrm{i}\,\mathbf{7.472}$	$\mathbf{1.166} \pm \mathrm{i}\,\mathbf{30.4}0$	$\mathbf{3}.019 \pm \mathrm{i}\,\mathbf{124}.8$	$\mathbf{6}.205 \pm \mathrm{i}\,\mathbf{506.3}^{*}$
400	$0.\mathbf{2021} \pm \mathrm{i}\,\mathbf{2.007}$	$0.\mathbf{2912} \pm \mathrm{i}\,\mathbf{7.4}91$	$\mathbf{1.223} \pm \mathrm{i}\,\mathbf{30.45}$	$\underline{3.148 \pm \mathrm{i}\,124.9^{*}}$	$\underline{6.595 \pm \mathrm{i}\,506.4^{\dagger}}$
1600	$\underline{0.2047 \pm \mathrm{i}\,2.010}$	$\underline{0.2974 \pm \mathrm{i}\,7.498}$	$\underline{1.234 \pm \mathrm{i}\,30.45^{*}}$	—	—
$10\pi^{\ddagger}$	$0.15 \pm \mathrm{i}\,2.0$	$0.4 \pm \mathrm{i}\,8.0$	$1.3 \pm \mathrm{i}\,32.0$	—	—
Bru.	$0.21 \pm \mathrm{i}\,1.94$	—	—	—	—
But.	$0.188 \pm \mathrm{i}\,1.955$	—	—	—	—

TABLE 5

Perturbed self-similar converging shock wave. Complex exponent values β of the shock-wave front deformation $\widetilde{d}_{\mathrm{s}}$ for each of the mode degrees $l = 4$, 16, 64, 256, 1024. Values established by a least-square fit of Eq. (39) with the shock-front deformation data as extracted from converging shock-wave computations. Results obtained with spatial grids of different uniform initial values of the number of cells per transverse wavelength — in effect $\mathfrak{N}^0 = 25$, 100, 400, 1600 — over the regions $10^{-3} \le r^0 \le 2$ (default), $10^{-2} \le r^0 \le 2$ (*), or $10^{-1} \le r^0 \le 2$ (†). The significant figures in agreement with the finest grid values (underlined) are indicated in bold. For comparison, the numerical exponent values (‡) — for $l = 4$, 16 and 64 — obtained in [8] with a linear perturbation artificial viscosity method and grids at $\mathfrak{N}^0 = 10\pi$ are reproduced, as well as the theoretical solution values for $l = 4$ given by (Bru.) Brushlinski (cited in [8]) and (But.) Butler [9, Tab. 1].

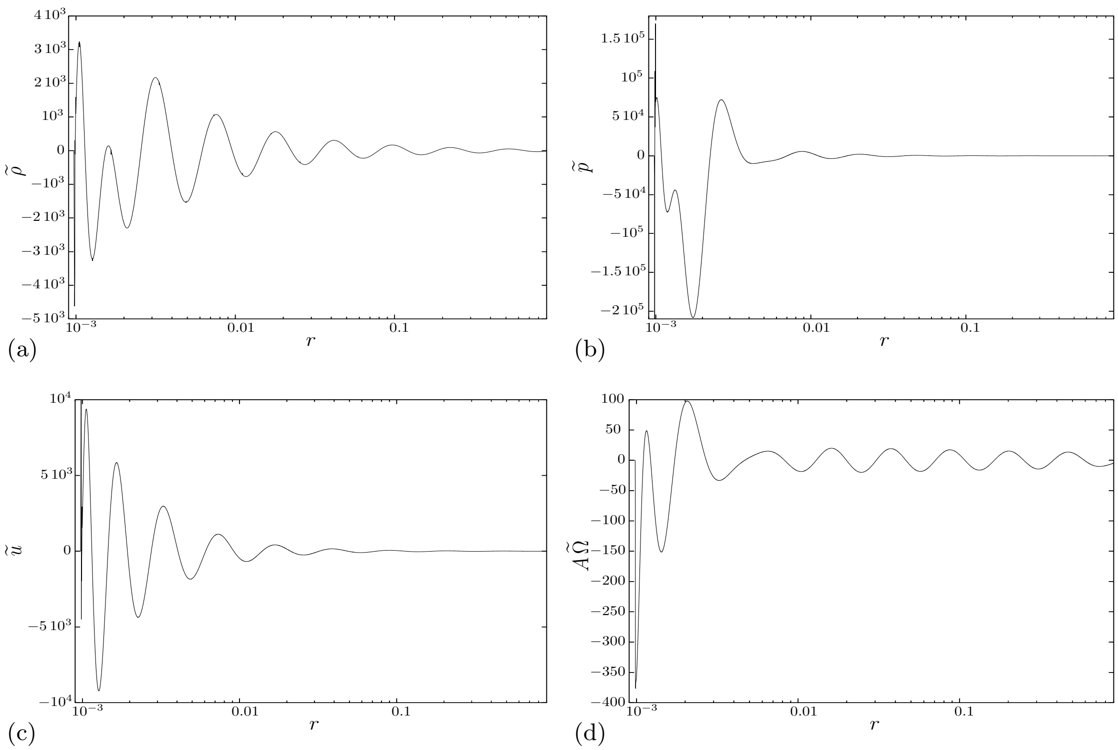

FIG. 7 Perturbed self-similar converging shock wave. Perturbation modal component profiles, for mode degree $l = 16$, of the (a) fluid density $\widetilde{\rho}$, (b) pressure $\widetilde{p}$, (c) fluid radial velocity $\widetilde{u}$, and (d) area lateral expansion $A\,\widetilde{\Omega}$, as functions of the radius r, by the time $r_{\mathrm{s}} \approx 10^{-3}$.

5. CONCLUSION

An explicit Godunov-type scheme for computing 3D linear perturbations of spherical radial flows of gas dynamics has been detailed. Four elements are constitutive of this scheme which proceeds from the works in [11] and [13], namely:

1. *Description of the perturbed flow motion in terms of linear Lagrangian perturbations [2, 33].* This choice not only allows, as for a multi-D Lagrangian description of flow motion, the sharp resolution of contact discontinuities but also, unlike purely Lagrangian multi-D numerical methods, the rendering of tangential velocity discontinuities. Besides, working with Lagrangian perturbations also simplifies the definition of initial conditions in that these may be chosen, for geometrically perturbed material discontinuities, in the class of functions (*e. g.* see [13, Sec.2 and App. C]) rather than — for the perturbation definitions of [39, 23, 22] also adopted in [35, 31] — in a class of measures (cf. [22, Sec. 5]).
2. *Basic-flow and perturbation numerical fluxes suitable for perturbed multi-material flow computations [13].* Here, the complete characterization of these fluxes in terms of elementary waves is provided by showing the equivalence between the linearized numerical flux and a linearization of the simple Riemann solver associated to the basic flow flux.
3. *Discrete formulation of the geometric conservation law for the motion perturbation.* Fully applying this principle stipulates the discretization of all the linear perturbation terms depending on the geometrical deformation field, thus ensuring mass (equivalently volume) conservation for the scheme. Consequently, modifications are brought to the scheme previously defined for planar-symmetric 1D flows in [13].
4. *Numerical stability analysis of the linear perturbation scheme.* Requirements bearing on the time-marching method for an explicit integration to be conditionally stable are formulated. A practical time-step constraint for numerical stability is provided in the case of third-order non-degenerate Runge–Kutta schemes, including that used in [13].

With these elements, the present Godunov-type method has been found to yield reliable quantitative results for strongly converging spherical flows whether they be isentropic compressions or collapsing shock waves. Perturbation result accuracy demands that a minimum number of grid cells per local transverse wavelength — values larger than 100 being recommended — be guaranteed throughout a computation. Such a requirement makes the overhead associated to the explicit treatment of perturbations marginal as compared to that of the basic-flow, thus limiting the eventual interest of a perturbation semi-implicit treatment as that of [31]. This requirement also imposes stringent constraints on grids for spherical systems since the cell size must be proportional to the radius and inversely proportional to the perturbation spherical harmonics degree, as previoulsy noted in [24, 44, 8]. Such constraints which should not be overlooked in multi-D simulations with equivalent schemes, make an accurate calculation of perturbed converging spherical flows at small perturbation scales, a particularly intensive computational task. This task could probably be lightened upon using adaptively refined grids in place of Lagrangian grids. Another characteristic of these computations is the inevitable inaccuracy of perturbation results about the origin of spherical systems due to the necessity of relaxing there the grid spatial sampling constraints. Nevertheless, linear perturbation computations, with Lagrangian grids, of shock-front collapses and rebounds have shown that practical guidelines could be formulated in such cases as examplified by extensive series of calculations carried out for ICF pellet type implosions: cf. [12].

The above approach to linear perturbation computation of gas dynamical flows sets the basis for extensions to other types of symmetries and fluid modelings, given that the method for deriving the perturbation PDEs and the different constitutive elements of the present Godunov-type scheme are of rather general scope. An illustration is provided by the extension of the present scheme to fluids with nonlinear heat conductions [4], leading to applications, in the context of ICF, of the perturbation code SILE$\mathcal{X}$: see [12].

The converging spherical shock-wave perturbation calculations reported in this paper clearly examplifies the interest of the linear perturbation computation approach in general and of the proposed scheme in particular, by producing shock-front deformation dynamics results which have yet to be matched by means of multi-D simulations. A broad scope of applications is available for this computational method, ranging from investigation of other hydrodynamic stability problems presenting similar characteristics — such as, for example, sonoluminescence [18] — or involving more complex phenomena — including flows encountered in ICF and astrophysics.

ACKNOWLEDGMENTS

The author wishes to thank Prof. P.-A. Raviart for stimulating discussions during the course of this work.

APPENDIX A: DERIVATION OF LINEAR LAGRANGIAN PERTURBATION EQUATIONS

This Appendix presents a derivation of the linear perturbation modal component equations (2), (4), (5) along the lines given at the beginning of Section 2.

A.1. Principles of the Lagrangian perturbation description

The principle of the Lagrangian perturbation description of a flow variation about its basic — or "unperturbed" — configuration consists in comparing the properties of the same fluid particle between the perturbed and unperturbed configurations: see [2, 33]. Assuming that initial or boundary data 3D perturbations of a solution to (1) depend on a single real parameter, say ε, with the convention that $\varepsilon = 0$ corresponds to the basic flow, this description amounts to studying, for any relevant fluid quantity X, the time evolution of its *Lagrangian perturbation*, that is the variable

$$\delta X_M(t;\varepsilon) = X_M(t;\varepsilon) - X_M(t;0), \tag{40}$$

defined for any fluid particle M. Such an approach evidently requires that, for ε in a neighborhood of $\varepsilon = 0$, the corresponding 3D perturbed flows exist and involve the same set of fluid particles. In particular, a Lagrangian system of coordinates, say $\left(\xi^1, \xi^2, \xi^3\right)$, whose definition is independent of the value of ε, must exist for this set of fluid particles. By designating, for any fluid quantity X, by the same symbol the corresponding function of $(\boldsymbol{\xi}, t; \varepsilon)$ where $\boldsymbol{\xi}$ stands for the coordinates $\left(\xi^1, \xi^2, \xi^3\right)$, we define *formally*, following [24], for any integer n, a nth-order Lagrangian perturbation operator $\mathbb{d}^n(.)$ as

$$\mathbb{d}^n : \ X\big(.,.;\varepsilon\big) \quad \longmapsto \quad \mathbb{d}^n X(.,.) = \left(\frac{\partial^n X}{\partial \varepsilon^n}(.,.;\varepsilon) \right) \Bigg|_{\varepsilon=0}. \tag{41}$$

The linear Lagrangian perturbation of a quantity X is then simply defined as $\mathbb{d}^1 X$ while its basic flow state corresponds to $\mathbb{d}^0 X$. When applying $\mathbb{d}^n(.)$ to any function of some arguments, the variables ξ^1, ξ^2, ξ^3, t and ε must be considered as independent variables, all other variables being taken as dependent. Hence the operator $\mathbb{d}^n(.)$ commutes with any partial differentiation with respect to the Lagrangian coordinates ξ^i, $1 \leq i \leq 3$, or t.

A.2. Linear Lagrangian perturbation equations in curvilinear coordinates

The equations for the linear Lagrangian perturbations of solutions to system (1) may be derived directly from considering the 3D gas dynamics equations, written in Lagrangian form and spherical coordinates, and applying the Lagrangian perturbation principles that we have just recalled. The corresponding algebra is however rather cumbersome. Another way of proceeding, as developed in [2, 7], consists in establishing the linear Lagrangian perturbation equations for an arbitrary system of coordinates, the results for spherical coordinates ensuing as a particular case. This is the approach we follow and summarize in this section.

Notations Let $\left(\eta^1,\eta^2,\eta^3\right)$ be a system of curvilinear coordinates for the Euclidean space and let $\left(\boldsymbol{\eta}_1,\boldsymbol{\eta}_2,\boldsymbol{\eta}_3\right)$ denote its vector basis. For such a coordinate system, we adopt the convention of [41] where superscripts and subscripts identify, respectively, *contravariant* and *covariant* quantities. Whence any vector $\boldsymbol{X}$ of the Euclidean space may be written as

$$\boldsymbol{X} = X^i\,\boldsymbol{\eta}_i = X_i\,\boldsymbol{\eta}^i,$$

where (X^i), $1\le i\le 3$, are the vector contravariant components, $\left(\boldsymbol{\eta}_1,\boldsymbol{\eta}_2,\boldsymbol{\eta}_3\right)$ is the covariant vector basis, while (X_i), $1\le i\le 3$, are the vector covariant components, and $\left(\boldsymbol{\eta}^1,\boldsymbol{\eta}^2,\boldsymbol{\eta}^3\right)$ the contravariant vector basis. (Throughout the rest of this Appendix, summation over a repeated index is always implied unless otherwise stated.) Recall that covariant and contravariant basis vectors are related through the identity

$$\boldsymbol{\eta}_i = g_{ij}\,\boldsymbol{\eta}^j,\quad 1\le i\le 3,$$

where (g_{ij}) denote the covariant components of the $\left(\eta^1,\eta^2,\eta^3\right)$-coordinate system metric tensor, i. e. the scalar products $g_{ij}=\boldsymbol{\eta}_i\cdot\boldsymbol{\eta}_j$. In addition, we shall also use the more compact notation $\boldsymbol{\eta}$ in place of the contravariant coordinates $\left(\eta^1,\eta^2,\eta^3\right)$ of an arbitrary point of the Euclidean space.

Lagrangian formulation of the equations of motion in curvilinear coordinates Given a curvilinear coordinate system $\left(\eta^1,\eta^2,\eta^3\right)$ whose definition *does not depend on the time variable t nor on the perturbation parameter ε*, and a Lagrangian coordinate system $\left(\xi^1,\xi^2,\xi^3\right)$ satisfying the requirements of Appendix A.1, we convene to use, for any function X of the variables $(\boldsymbol{\xi},t;\varepsilon)$, the notation $\overline{X}$ to designate the function of $(\boldsymbol{\eta},t;\varepsilon)$ defined by

$$\overline{X}\big(\boldsymbol{\eta}(\boldsymbol{\xi},t;\varepsilon),t;\varepsilon\big) \stackrel{\text{def}}{=} X(\boldsymbol{\xi},t;\varepsilon).$$

With this convention, the 3D gas dynamics equations in the absence of massic forces may be written, according to a Lagrangian description of the fluid particle motion, as

$$\partial_t\tau - \tau\,\nabla_i\overline{u^i} = 0, \tag{42a}$$

$$\big(\partial_t\boldsymbol{u}\big)_i + \tau\,\nabla_i\overline{p} = 0,\quad 1\le i\le 3, \tag{42b}$$

$$\partial_t e + \tau\,\nabla_i\overline{p\,u^i} = 0, \tag{42c}$$

$$\partial_t\eta^i = u^i,\quad 1\le i\le 3. \tag{42d}$$

In these equations, the notation $\nabla_i\overline{X^i}$ stands for the expression, in the $\left(\eta^1,\eta^2,\eta^3\right)$-coordinate system, of the divergence $\operatorname{div}\boldsymbol{X}$ of a vector field $\boldsymbol{X}$, namely

$$\nabla_i\overline{X^i} \equiv \frac{1}{J_{\boldsymbol{\eta}}}\,\partial_{\eta^i}\big(J_{\boldsymbol{\eta}}\,\overline{X^i}\big) = \partial_{\xi^j}X^i\,\frac{\partial\xi^j}{\partial\eta^i} + \big(\partial_{\eta^i}\ln J_{\boldsymbol{\eta}}\big)\,X^i, \tag{43}$$

with the notation $J_{\boldsymbol{\eta}} = \det\!\big(\partial x^i/\partial\eta^j\big) = \sqrt{\det(g_{ij})}$, while $\nabla_i\overline{X}$ stands for the expression, in the same coordinate system, of the ith covariant component of the gradient of a scalar field X, $(\mathbf{grad}\,X)_i$, i. e. the covariant derivative

$$\nabla_i\overline{X} \equiv \partial_{\eta^i}\overline{X} = \partial_{\xi^j}X\,\frac{\partial\xi^j}{\partial\eta^i}, \tag{44}$$

e. g. see [41]. In Eq. (42b), the *covariant* components of $\partial_t\boldsymbol{u}$, the particle acceleration, are usually obtained by means of Lagrange's formulas

$$a_i = \big(\partial_t\boldsymbol{u}\big)_i = \frac{d}{dt}\big[\partial_{\dot\eta^i}K(\boldsymbol{\eta},\dot{\boldsymbol{\eta}},t)\big] - \partial_{\eta^i}K(\boldsymbol{\eta},\dot{\boldsymbol{\eta}},t),\quad 1\le i\le 3, \tag{45}$$

with the notations $\dot\eta^i = \partial_t\eta^i$, $\dot{\boldsymbol{\eta}} = \left(\dot\eta^1,\dot\eta^2,\dot\eta^3\right)$, and where $K(\boldsymbol{\eta},\dot{\boldsymbol{\eta}},t)$ stands for the expression, explicit in the variables $(\boldsymbol{\eta},\dot{\boldsymbol{\eta}},t)$, of the fluid specific kinetic energy $K = e - \mathcal{E}$. Since in the present case, the definition of the (η^1, η^2, η^3)-coordinate system is independent of t, this kinetic energy reduces to the standard definition

$$K = \frac{1}{2}\, g_{ij}\, \dot{\eta}^i\, \dot{\eta}^j = \frac{1}{2}\, \boldsymbol{u} \cdot \boldsymbol{u}. \tag{46}$$

Using this expression in Eq. (45) requires in turn knowing the explicit formulas, in terms of the variables η^k and $\dot{\eta}^k$, for the tensor components g_{ij} — formulas which are only available once the curvilinear coordinate system has been specified.

Independently of the system of equations (42), a first integral of Eq. (42a) is provided by the conservation of mass applied to an infinitesimal fluid element. By letting $J_{\boldsymbol{\xi}} = \det(\partial x^i/\partial \xi^j)$ denote the Jacobian of the transformation $\boldsymbol{\xi} \mapsto \boldsymbol{x}$, this first integral taken at the point $\boldsymbol{\xi}$ may be written as

$$\rho(\boldsymbol{\xi}, t; \varepsilon)\, J_{\boldsymbol{\xi}}(\boldsymbol{\xi}, t; \varepsilon) = \rho_\star(\boldsymbol{\xi}), \tag{47}$$

where $\rho_\star$ stands for the fluid density in some reference state — possibly virtual — of the fluids under consideration for which $J_{\boldsymbol{\xi}} = 1$. Naturally this equation holds at any point $\boldsymbol{\xi}$ where the transformation $\boldsymbol{\xi} \mapsto \boldsymbol{x}$ is a diffeomorphism, whatever (t, ε). Note that the independence of $\rho_\star$ with respect to the parameter ε is a consequence of requiring the definition of the Lagrangian coordinate system (ξ^1, ξ^2, ξ^3) to be independent of ε.

System (42) and equation (47) constitute the main equations for obtaining the linear Lagrangian perturbation formulation of the fluid motion equations.

A.2.1. Properties of linear Lagrangian perturbations

Prior to establishing the linear Lagrangian perturbations of Eqs. (42), (47), we recall certain general properties of linear Lagrangian perturbations. For the sake of completeness, these properties, listed below as Propositions 1–3, are produced with their proofs, using the conventions retained in this paper. Note that more or less equivalent formulations of these propositions have already been given in the same context of curvilinear coordinates. Hence Proposition 1 is implied by [2, § 75, Eq. (12)], while Proposition 2 appears as (*ibid.*, § 75, Eq. (15) along with § 18, Eq. (10)). As for Proposition 3, a slightly different form is found in [7, Eq. (3.16)].

Proposition 1. *The linear Lagrangian perturbation of $J_{\boldsymbol{\xi}}$, the Jacobian of the transformation $\boldsymbol{\xi} \mapsto \boldsymbol{x}$, reads*

$$\mathbb{d}^1 J_{\boldsymbol{\xi}} = \mathbb{d}^0 J_{\boldsymbol{\xi}}\, \nabla_i \overline{\mathbb{d}^1 \eta^i}. \tag{48}$$

Proof. By definition of $J_{\boldsymbol{\xi}}$, we have

$$\mathbb{d}^1 J_{\boldsymbol{\xi}} = \mathbb{d}^1 \left(\det\Big(\frac{\partial x^i}{\partial \xi^j}\Big) \right) = \mathbb{d}^0 \big(J_{\boldsymbol{\xi}}\big)_{kl}\; \mathbb{d}^1 \Big(\frac{\partial x^k}{\partial \xi^l}\Big) = \big(\mathbb{d}^0 J_{\boldsymbol{\xi}}\big)_{kl}\, \frac{\partial\, \mathbb{d}^1 x^k}{\partial \xi^l},$$

where $\big(J_{\boldsymbol{\xi}}\big)_{kl}$ denotes the cofactor of $\partial x^k/\partial \xi^l$ in the expression of $\det\big(\partial x^i/\partial \xi^j\big)$. Then, upon expanding $\partial\, \mathbb{d}^1 x^k/\partial \xi^l$ as

$$\frac{\partial\, \mathbb{d}^1 x^k}{\partial \xi^l} = \frac{\partial\, \mathbb{d}^1 x^k}{\partial \xi^m}\; \mathbb{d}^0 \Big(\frac{\partial \xi^m}{\partial x^n}\Big)\, \frac{\partial\, \mathbb{d}^0 x^n}{\partial \xi^l},$$

it comes that

$$\mathbb{d}^1 J_{\boldsymbol{\xi}} = \big(\mathbb{d}^0 J_{\boldsymbol{\xi}}\big)_{kl} \frac{\partial\, \mathbb{d}^0 x^n}{\partial \xi^l}\, \frac{\partial\, \mathbb{d}^1 x^k}{\partial \xi^m}\; \mathbb{d}^0 \Big(\frac{\partial \xi^m}{\partial x^n}\Big).$$

From the fact that

$$\big(\mathbb{d}^0 J_{\boldsymbol{\xi}}\big)_{kl} \frac{\partial\, \mathbb{d}^0 x^n}{\partial \xi^l} = \mathbb{d}^0 J_{\boldsymbol{\xi}}\, \delta_{kn},$$

where δ_{kn} is Kronecker's symbol, we infer that

$$\mathbb{d}^1 J_{\boldsymbol{\xi}} = \mathbb{d}^0 J_{\boldsymbol{\xi}}\, \frac{\partial\, \mathbb{d}^1 x^k}{\partial \xi^m}\; \mathbb{d}^0 \Big(\frac{\partial \xi^m}{\partial x^k}\Big).$$

Having noted that

$$\frac{\partial\, \mathrm{d}^1 x^k}{\partial \xi^m}\ \mathrm{d}^0\Big(\frac{\partial \xi^m}{\partial x^k}\Big) = \mathrm{div}\,\big(\,\mathrm{d}^1 x^i\, \boldsymbol{x}_i\big) = \mathrm{div}\,\big(\,\mathrm{d}^1 \eta^i\, \boldsymbol{\eta}_i\big) = \nabla_i \overline{\mathrm{d}^1 \eta^i},$$

since $\mathrm{d}^1 x^i\, \boldsymbol{x}_i = \mathrm{d}^1 \eta^i\, \boldsymbol{\eta}_i$, we immediately get Eq. (48). ∎

Proposition 2. *Given a scalar function X of the variables $(\boldsymbol{\xi}, t; \varepsilon)$, its covariant derivative linear Lagrangian perturbations are*

$$\mathrm{d}^1\big(\nabla_i \overline{X}\big) = \nabla_i \overline{\mathrm{d}^1 X} - \nabla_k \overline{\mathrm{d}^0 X}\, \nabla_i \overline{\mathrm{d}^1 \eta^k}, \quad 1 \le i \le 3. \tag{49}$$

Proof. From the expression (44) of $\nabla_i \overline{X}$, it comes that

$$\mathrm{d}^1\big(\nabla_i \overline{X}\big) = \partial_{\xi^j}\ \mathrm{d}^1 X\ \mathrm{d}^0\Big(\frac{\partial \xi^j}{\partial \eta^i}\Big) + \partial_{\xi^j}\ \mathrm{d}^0 X\ \mathrm{d}^1\Big(\frac{\partial \xi^j}{\partial \eta^i}\Big) = \nabla_i \overline{\mathrm{d}^1 X} + \partial_{\xi^j}\ \mathrm{d}^0 X\ \mathrm{d}^1\Big(\frac{\partial \xi^j}{\partial \eta^i}\Big). \tag{50}$$

Independently of this result, we deduce from the equality

$$\frac{\partial \xi^j}{\partial \eta^k}\, \frac{\partial \eta^k}{\partial \xi^l} = \delta_{jl}$$

which holds regardless of the value of ε, that

$$\mathrm{d}^1\Big(\frac{\partial \xi^j}{\partial \eta^k}\Big)\ \mathrm{d}^0\Big(\frac{\partial \eta^k}{\partial \xi^l}\Big) + \mathrm{d}^0\Big(\frac{\partial \xi^j}{\partial \eta^k}\Big)\ \mathrm{d}^1\Big(\frac{\partial \eta^k}{\partial \xi^l}\Big) = 0.$$

Multiplying this identity by $\mathrm{d}^0\big(\partial \xi^l / \partial \eta^m\big)$ and summing over the index l, yields

$$\mathrm{d}^1\Big(\frac{\partial \xi^j}{\partial \eta^k}\Big)\, \delta_{km} + \mathrm{d}^0\Big(\frac{\partial \xi^j}{\partial \eta^k}\Big)\ \mathrm{d}^1\Big(\frac{\partial \eta^k}{\partial \xi^l}\Big)\ \mathrm{d}^0\Big(\frac{\partial \xi^l}{\partial \eta^m}\Big) = 0,$$

whence

$$\mathrm{d}^1\Big(\frac{\partial \xi^j}{\partial \eta^i}\Big) = -\,\mathrm{d}^0\Big(\frac{\partial \xi^j}{\partial \eta^k}\Big)\, \frac{\partial\, \mathrm{d}^1 \eta^k}{\partial \xi^l}\ \mathrm{d}^0\Big(\frac{\partial \xi^l}{\partial \eta^i}\Big) = -\,\mathrm{d}^0\Big(\frac{\partial \xi^j}{\partial \eta^k}\Big)\, \nabla_i \overline{\mathrm{d}^1 \eta^k}, \tag{51}$$

where we have used the expression (44) of $\nabla_i \overline{X}$ with $X = \mathrm{d}^1 \eta^k$. Substituting this result in Eq. (50) and noticing that

$$\partial_{\xi^j}\ \mathrm{d}^0 X\ \mathrm{d}^0\Big(\frac{\partial \xi^j}{\partial \eta^k}\Big) = \nabla_k \overline{\mathrm{d}^0 X},$$

yields Eq. (49). ∎

Proposition 3. *Given a vector function $\boldsymbol{X}$ of the variables $(\boldsymbol{\xi}, t; \varepsilon)$, its divergence linear Lagrangian perturbation comes as*

$$\mathrm{d}^1\big(\nabla_i \overline{X^i}\big) = \nabla_i \overline{\mathrm{d}^1 X^i} - \nabla_k \overline{\mathrm{d}^0 X^i}\, \nabla_i \overline{\mathrm{d}^1 \eta^k} + \mathrm{d}^0 X^i\ \big(\partial^2_{\eta^i \eta^j} \ln J_{\boldsymbol{\eta}}\big)\Big|_{\mathrm{d}^0 \boldsymbol{\eta}}\ \mathrm{d}^1 \eta^j. \tag{52}$$

Proof. Applying $\mathrm{d}^1(.)$ to the definition (43) of $\nabla_i \overline{X^i}$ yields

$$\mathrm{d}^1\big(\nabla_i \overline{X^i}\big) = \partial_{\xi^j}\ \mathrm{d}^1 X^i\ \mathrm{d}^0\Big(\frac{\partial \xi^j}{\partial \eta^i}\Big) + \mathrm{d}^0\big(\partial_{\eta^i} \ln J_{\boldsymbol{\eta}}\big)\ \mathrm{d}^1 X^i + \partial_{\xi^j}\ \mathrm{d}^0 X^i\ \mathrm{d}^1\Big(\frac{\partial \xi^j}{\partial \eta^i}\Big) + \mathrm{d}^1\big(\partial_{\eta^i} \ln J_{\boldsymbol{\eta}}\big)\ \mathrm{d}^0 X^i. \tag{53}$$

Since $J_{\boldsymbol{\eta}}$ is a function of the sole variables $\big(\eta^1, \eta^2, \eta^3\big)$, it follows that

$$\mathrm{d}^0\big(\partial_{\eta^i} \ln J_{\boldsymbol{\eta}}\big) = \big(\partial_{\eta^i} \ln J_{\boldsymbol{\eta}}\big)\Big|_{\mathrm{d}^0 \boldsymbol{\eta}}, \qquad \mathrm{d}^1\big(\partial_{\eta^i} \ln J_{\boldsymbol{\eta}}\big) = \big(\partial^2_{\eta^j \eta^i} \ln J_{\boldsymbol{\eta}}\big)\Big|_{\mathrm{d}^0 \boldsymbol{\eta}}\ \mathrm{d}^1 \eta^j.$$

Whence Eq. (53) reads

$$\mathbb{d}^1\big(\nabla_i\overline{X^i}\big) = \underbrace{\partial_{\xi^j}\,\mathbb{d}^1X^i\;\mathbb{d}^0\Big(\frac{\partial\xi^j}{\partial\eta^i}\Big) + \big(\partial_{\eta^i}\ln J_{\boldsymbol{\eta}}\big)\big|_{\mathbb{d}^0\boldsymbol{\eta}}\,\mathbb{d}^1X^i}_{=\nabla_i\overline{\mathbb{d}^1X^i}}$$
$$+\,\partial_{\xi^j}\,\mathbb{d}^0X^i\;\mathbb{d}^1\Big(\frac{\partial\xi^j}{\partial\eta^i}\Big) + \mathbb{d}^0X^i\,\big(\partial^2_{\eta^i\eta^j}\ln J_{\boldsymbol{\eta}}\big)\Big|_{\mathbb{d}^0\boldsymbol{\eta}}\,\mathbb{d}^1\eta^j,$$

which, upon using Eq. (51), leads to the proposed result. ∎

A.2.2. Linear Lagrangian perturbation equations

Within the formalism introduced in Appendix A.1, the equations for the motion linear Lagrangian perturbations may be derived formally upon applying the operator $\mathbb{d}^1(.)$ to Eqs. (42), (47). The case of the fluid particle trajectory equations (42d) is immediate, yielding the contravariant component equations

$$\partial_t\,\mathbb{d}^1\eta^i = \mathbb{d}^1u^i = \mathbb{d}^1\dot\eta^i,\quad 1\le i\le 3. \tag{54}$$

As for the remaining equations of (42), (47), their linearization proceeds from the results stated in Propositions 4–6 below.

Proposition 4 (Mass conservation). *The linear Lagrangian perturbation of the mass conservation equation* (47) *comes as (cf. [2, § 75, Eq. (12)])*

$$\mathbb{d}^1\tau = \mathbb{d}^0\tau\,\nabla_i\overline{\mathbb{d}^1\eta^i}. \tag{55}$$

This formulation of the mass conservation equation linear perturbation is derived, with the help of Proposition 1, by applying $\mathbb{d}^1(.)$ to Eq. (47), having noted that $\rho_\star$ does not depend on ε.

Proposition 5 (Scalar conservation laws). *The linear Lagrangian perturbation of a scalar conservation law of the form*

$$\partial_tX + \tau\,\nabla_i\overline{\Phi^i} = 0, \tag{56}$$

reads

$$\partial_t\,\mathbb{d}^1X + \mathbb{d}^0\tau\Big(\nabla_i\overline{\mathbb{d}^1\Phi^i} + \nabla_i\overline{\mathbb{d}^0\Phi^i}\,\nabla_i\overline{\mathbb{d}^1\eta^i} - \nabla_k\overline{\mathbb{d}^0\Phi^i}\,\nabla_i\overline{\mathbb{d}^1\eta^k} + \mathbb{d}^0\Phi^i\,\big(\partial^2_{\eta^i\eta^j}\ln J_{\boldsymbol{\eta}}\big)\Big|_{\mathbb{d}^0\boldsymbol{\eta}}\,\mathbb{d}^1\eta^j\Big) = 0. \tag{57}$$

This result simply follows from applying $\mathbb{d}^1(.)$ to Eq. (56) and using both Proposition 3 and Proposition 4.

Remark 4. Such a formulation of the linear Lagrangian perturbation of a scalar conservation law in an arbitrary curvilinear coordinate system does not seem to have been previously established. Indeed the earlier works of [2, 7] relied on non-conservative formulations of the gas dynamics equations, while the more recent conservative formulations of [11, 13] are specific to Cartesian or spherical coordinates while those found in [39, 31] pertain, in addition, to a different kind of linear perturbations.

Proposition 6 (Acceleration covariant component equations). *The linear Lagrangian perturbations of the acceleration component equations* (42b) *are given by*

$$\mathbb{d}^1a_i + \mathbb{d}^0\tau\,\Big(\nabla_i\overline{\mathbb{d}^1p} + \nabla_i\overline{\mathbb{d}^0p}\,\nabla_j\overline{\mathbb{d}^1\eta^j} - \nabla_j\overline{\mathbb{d}^0p}\,\nabla_i\overline{\mathbb{d}^1\eta^j}\Big) = 0,\quad 1\le i\le 3, \tag{58}$$

with the notations of Eq. (45).

This formulation of the acceleration linear perturbation covariant component equations is readily obtained from Eq. (55) and Proposition 2. Naturally, deriving expressions — after Lagrange's formulas (45) along with Eq. (46) — for the acceleration linear perturbation covariant components, $\mathbb{d}^1 a_i$, can only be achieved once the curvilinear coordinate system has been entirely specified. Nevertheless, this coordinate system being, by assumption, independent of ε, we have the general formula [2, § 75, Eq. (10)]

$$\mathbb{d}^1\big[K(\boldsymbol{\eta},\dot{\boldsymbol{\eta}},t)\big] = \partial_{\eta^i} K\big(\mathbb{d}^0\boldsymbol{\eta},\mathbb{d}^0\dot{\boldsymbol{\eta}},t\big)\ \mathbb{d}^1\eta^i + \partial_{\dot{\eta}^i} K\big(\mathbb{d}^0\boldsymbol{\eta},\mathbb{d}^0\dot{\boldsymbol{\eta}},t\big)\ \mathbb{d}^1\dot{\eta}^i. \tag{59}$$

Remark 5. Let us mention that equations almost identical to Eq. (58) are given in [7, Eq. (3.9)]. Other formulations for the fluid particle acceleration perturbation equations could equally be considered. Nevertheless, the covariant component formulation of Eq. (58) turns out to be preferable — in terms of simplicity of the expressions — over a contravariant formulation. The same is true as for the relative merit of a component form over a vector form for these equations, the latter choice leading to more complicated systems of equations.

Given the above results, the complete set of equations for the motion linear Lagrangian perturbations consists in Eqs. (54), (55), (58) along with those resulting from applying Proposition 5 to the equations for the specific volume (42a) and total energy (42c), augmented by the linearized form of the fluid equations of state, i. e.

$$\mathbb{d}^1 p = P_\tau\big(\mathbb{d}^0\tau,\mathbb{d}^0\mathcal{E}\big)\ \mathbb{d}^1\tau + P_{\mathcal{E}}\big(\mathbb{d}^0\tau,\mathbb{d}^0\mathcal{E}\big)\ \mathbb{d}^1\mathcal{E}, \tag{60}$$

with the notations of Eq. (6) and, for the specific internal energy perturbation, $\mathbb{d}^1\mathcal{E} = \mathbb{d}^1 e - \mathbb{d}^1 K$ where $\mathbb{d}^1 K$ is deduced from Eq. (59). Let us emphasize that if, in Cartesian coordinates, one can recast the corresponding evolution equations for the specific volume, velocity components, and total energy linear perturbations into a system of conservation laws (*e. g.* see [13]), this is not necessarily the case for arbitrary curvilinear coordinates.

A.3. Radial basic flows with spherical symmetry

We now go back to the configuration which is of primary interest to us, namely that of basic flows which are solutions to (1).

A.3.1. Definitions of the curvilinear and Lagrangian coordinate systems

The symmetry of the basic solutions evidently suggests relying on the usual spherical coordinates (r,θ,φ) when defining the $\big(\eta^1,\eta^2,\eta^3\big)$-coordinate system. A certain amount of freedom exists however in the definition of the contravariant coordinates $\big(\eta^1,\eta^2,\eta^3\big)$. Here, as in [7], we retain the simplest choice $\big(\eta^1,\eta^2,\eta^3\big) \equiv (r,\theta,\varphi)$. Consequently, the covariant vector basis is $\big(\boldsymbol{\eta}_1,\boldsymbol{\eta}_2,\boldsymbol{\eta}_3\big) = \big(\boldsymbol{e}_r, r\,\boldsymbol{e}_\theta, r\,\sin\theta\,\boldsymbol{e}_\varphi\big)$, where $\big(\boldsymbol{e}_r,\boldsymbol{e}_\theta,\boldsymbol{e}_\varphi\big)$ is the usual spherical coordinate system orthonormal vector basis. The $\big(\eta^1,\eta^2,\eta^3\big)$-coordinate system metric tensor is then

$$\big(g_{ij}\big) = \begin{pmatrix} 1 & 0 & 0 \\ 0 & r^2 & 0 \\ 0 & 0 & r^2\sin^2\theta \end{pmatrix}, \tag{61}$$

while the Jacobian $J_{\boldsymbol{\eta}}$ amounts to $J_{\boldsymbol{\eta}} = r^2\,\sin\theta$. In particular, the basic flow radial motions are characterized by the equations

$$\mathbb{d}^0\eta^2 \equiv \mathbb{d}^0\theta = \text{cst} \quad \text{and} \quad \mathbb{d}^0\eta^3 \equiv \mathbb{d}^0\varphi = \text{cst}.$$

This last feature leads us to define the Lagrangian coordinate system as being $\big(\xi^1,\xi^2,\xi^3\big) \equiv \big(m,\mathbb{d}^0\theta,\mathbb{d}^0\varphi\big)$ where m is the Lagrangian coordinate used in the basic flow system of equations (1). With such a choice, the Jacobian matrix of the coordinate transformation $\boldsymbol{\eta} \mapsto \boldsymbol{\xi}$, for $\varepsilon = 0$, is

$$\left(\mathbb{d}^0\Big(\frac{\partial\xi^i}{\partial\eta^j}\Big)\right) = \begin{pmatrix} \mathbb{d}^0\rho\,\mathbb{d}^0 r^2 & 0 & 0 \\ 0 & 1 & 0 \\ 0 & 0 & 1 \end{pmatrix}. \tag{62}$$

In addition to these definitions, we introduce the notations

$$\boldsymbol{X}_\perp = \left\{X^i\,\boldsymbol{\eta}_i\right\}_{i\neq 1}, \quad \operatorname{div}_\perp \boldsymbol{X}_\perp = \left\{\nabla_i X^i\right\}_{i\neq 1}, \tag{63}$$

for any vector field $\boldsymbol{X}$, and

$$\mathbf{grad}_\perp X = \left\{\nabla_i X\,\boldsymbol{\eta}^i\right\}_{i\neq 1}, \tag{64}$$

for any scalar field X, and convene to use, in the sequel, the notation r in place of η^1 while keeping the index notations for the other curvilinear coordinates.

A.3.2. Linear Lagrangian perturbation equations

Given the assumptions and the definitions of Sec. A.3.1, we have

PROPOSITION 7. *For spherically-symmetric radial basic flows, the linear Lagrangian perturbation of the system of gas dynamics* (42) *may be written as the system of linear perturbation equations*

$$\begin{aligned}
&\partial_t\,\mathbb{d}^1\tau - \partial_m\big(\mathbb{d}^0 A\;\mathbb{d}^1 u^1\big) - \mathbb{d}^0\tau\;\operatorname{div}_\perp \mathbb{d}^1\boldsymbol{u}_\perp - \partial_m\big(\mathbb{d}^1 A\;\mathbb{d}^0 u^1\big)\\
&\qquad\qquad\qquad - \partial_m\big(\mathbb{d}^0 A\;\mathbb{d}^0 u^1\big)\;\operatorname{div}_\perp \mathbb{d}^1\boldsymbol{\eta}_\perp = 0,
\end{aligned} \tag{65a}$$

$$\begin{aligned}
&\partial_t\,\mathbb{d}^1 u^1 + \partial_m\big(\mathbb{d}^0 A\;\mathbb{d}^1 p\big) + \partial_m\big(\mathbb{d}^1 A\;\mathbb{d}^0 p\big) + \partial_m\big(\mathbb{d}^0 A\;\mathbb{d}^0 p\big)\;\operatorname{div}_\perp \mathbb{d}^1\boldsymbol{\eta}_\perp\\
&\qquad\qquad - \mathbb{d}^1 p\,\partial_m\,\mathbb{d}^0 A - \mathbb{d}^0 p\,\big(\partial_m\,\mathbb{d}^1 A + \partial_m\,\mathbb{d}^0 A\;\operatorname{div}_\perp \mathbb{d}^1\boldsymbol{\eta}_\perp\big) = 0,
\end{aligned} \tag{65b}$$

$$\begin{aligned}
&\left\{\frac{d}{dt}\Big[\big(g_{kk}|_{\mathbb{d}^0\boldsymbol{\eta}}\;\mathbb{d}^1 u^k\big)_{k=i}\Big]\boldsymbol{\eta}^i\right\}_{i\neq 1} + \mathbb{d}^0\tau\;\mathbf{grad}_\perp\,\mathbb{d}^1 p\\
&\qquad\qquad + \Big[\mathbb{d}^0 p\,\partial_m\,\mathbb{d}^0 A - \partial_m\big(\mathbb{d}^0 A\;\mathbb{d}^0 p\big)\Big]\;\mathbf{grad}_\perp\,\mathbb{d}^1 r = \mathbf{0},
\end{aligned} \tag{65c}$$

$$\begin{aligned}
&\partial_t\,\mathbb{d}^1 e + \partial_m\big[\mathbb{d}^0 A\;\mathbb{d}^1(p\,u^1)\big] + \mathbb{d}^0\tau\;\mathbb{d}^0 p\;\operatorname{div}_\perp \mathbb{d}^1\boldsymbol{u}_\perp + \partial_m\big(\mathbb{d}^1 A\;\mathbb{d}^0 p\;\mathbb{d}^0 u^1\big)\\
&\qquad\qquad + \partial_m\big(\mathbb{d}^0 A\;\mathbb{d}^0 p\;\mathbb{d}^0 u^1\big)\;\operatorname{div}_\perp \mathbb{d}^1\boldsymbol{\eta}_\perp = 0,
\end{aligned} \tag{65d}$$

$$\partial_t\,\mathbb{d}^1 r = \mathbb{d}^1 u^1, \quad \textit{and} \quad \partial_t\,\mathbb{d}^1\eta^i = \mathbb{d}^1 u^i, \quad i\neq 1, \tag{65e}$$

completed by the fluid linearized equations of state (60)*, wherein* $\mathbb{d}^1\mathcal{E} = \mathbb{d}^1 e - \mathbb{d}^0 u^1\;\mathbb{d}^1 u^1$*, and the linear Lagrangian perturbation of the mass conservation equation* (47) *under the form*

$$\mathbb{d}^1\tau = \partial_m\big(\mathbb{d}^0 A\;\mathbb{d}^1 r\big) + \mathbb{d}^0\tau\;\operatorname{div}_\perp \mathbb{d}^1\boldsymbol{\eta}_\perp, \tag{66}$$

where A is the area involved in Eq. (1)*.*

Proof. The above formulation (65), (66) of the linear perturbation equation is derived having in mind the specific form of the system of equations (1) and performing the change of independent variables $\big(\eta^1,\eta^2,\eta^3\big) \to \big(m,\mathbb{d}^0\theta,\mathbb{d}^0\varphi\big)$.

Starting with the scalar conservation law perturbation (57), we note that the basic flow properties along with Eq. (62) lead to the following simplifications:

$$\nabla_k\overline{\mathbb{d}^0\Phi^i}\;\nabla_i\overline{\mathbb{d}^1\eta^k} = \big(\mathbb{d}^0\rho\;\mathbb{d}^0 A\big)^2\;\partial_m\,\mathbb{d}^0\Phi^1\,\partial_m\,\mathbb{d}^1 r,$$

by means of expression (44) for the covariant derivatives, and

$$\nabla_i\overline{\mathbb{d}^0\Phi^i} = \mathbb{d}^0\rho\,\partial_m\big(\mathbb{d}^0 A\;\mathbb{d}^0\Phi^1\big)\,,$$

since $\big(\partial_r \ln J_{\boldsymbol{\eta}}\big)\big|_{\mathbb{d}^0\boldsymbol{\eta}} = \mathbb{d}^0\rho\,\partial_m\,\mathbb{d}^0 A$. Further simplifications are also brought up by the definition of the $\big(\eta^1,\eta^2,\eta^3\big)$-coordinate system itself. Hence, the definition of $J_{\boldsymbol{\eta}}$ induces that

$$\partial^2_{\eta^i r}\ln J_{\boldsymbol{\eta}} = 0, \quad \text{for } i\neq 1, \tag{67}$$

and therefore that

$$\mathbb{d}^0\Phi^i \left(\partial^2_{\eta^i\eta^j} \ln J_{\boldsymbol{\eta}}\right)\Big|_{\mathbb{d}^0\boldsymbol{\eta}} \mathbb{d}^1\eta^j = -\frac{2}{\mathbb{d}^0 A}\, \mathbb{d}^0\Phi^1\, \mathbb{d}^1 r.$$

Taking advantage of these results, a significant amount of manipulations and the use of the relations

$$\mathbb{d}^0\rho\, \partial_m\, \mathbb{d}^0 A = \frac{2}{\mathbb{d}^0 r}, \qquad \text{and} \qquad \mathbb{d}^0\rho\, \partial_m\, \mathbb{d}^0 r = \frac{1}{\mathbb{d}^0 A},$$

in Eq. (57), leads to the equation

$$\partial_t\, \mathbb{d}^1 X + \partial_m\big(\mathbb{d}^0 A\; \mathbb{d}^1\Phi^1\big) + \mathbb{d}^0\tau\; \mathrm{div}_\perp\, \mathbb{d}^1\boldsymbol{\Phi}_\perp + \partial_m\big(\mathbb{d}^1 A\; \mathbb{d}^0\Phi^1\big) \\ + \partial_m\big(\mathbb{d}^0 A\; \mathbb{d}^0\Phi^1\big)\; \mathrm{div}_\perp\, \mathbb{d}^1\boldsymbol{\eta}_\perp = 0, \quad (68)$$

where, by definition, $\mathbb{d}^1 A = 2\,\mathbb{d}^0 r\,\mathbb{d}^1 r$. The conservation law perturbations for the specific volume τ and total energy e, namely Eqs. (65a) and (65d), follow then immediately upon performing, in the above equation, the substitutions $(X, \boldsymbol{\Phi}) \to (\tau, \boldsymbol{u})$ and $(X, \boldsymbol{\Phi}) \to (e, p\boldsymbol{u})$, respectively.

The equations for the radial and orthoradial acceleration linear perturbations (65b) and (65c) are deduced from Eq. (58) thanks to the fact that

$$\nabla_j \overline{\mathbb{d}^0 p}\, \nabla_i \overline{\mathbb{d}^1\eta^j} = \mathbb{d}^0\rho\; \mathbb{d}^0 A\, \partial_m\, \mathbb{d}^0 p\, \nabla_i \overline{\mathbb{d}^1 r}, \quad i \le i \le 3,$$

and

$$\mathbb{d}^1 a_1 = \partial_t\, \mathbb{d}^1 u^1, \quad \text{and} \quad \mathbb{d}^1 a_i = \frac{d}{dt}\Big[\big(g_{kk}|_{\mathbb{d}^0\boldsymbol{\eta}}\; \mathbb{d}^1 u^k\big)_{k=i}\Big], \quad i \neq 1,$$

which stem from Eqs. (45), (46) and (59).

Finally, Eqs. (65e) and (66) are simply Eqs. (54) and (55) written with the newly introduced conventions. ∎

Remark 6. The particular form of Eqs. (65) and (66) has been chosen based on the conservative formulation (1) of the system of equations for the basic flow. In that respect, this form differs from formulations that could be derived in a more direct way from Eqs. (57) and (58). Nevertheless, whatever the formulation that is retained, the resulting equations present the interesting feature that the motion perturbation in the plane defined by $(\boldsymbol{\eta}_2, \boldsymbol{\eta}_3)$ — or *transverse plane* — only appears in Eqs. (65a), (65b), (65d), (66) by means of the transverse divergence terms $\mathrm{div}_\perp\, \mathbb{d}^1\boldsymbol{\eta}_\perp$ and $\mathrm{div}_\perp\, \mathbb{d}^1\boldsymbol{u}_\perp$. This peculiarity quite naturally suggests performing a Helmholtz decomposition of the transverse Lagrangian displacement perturbation field $\mathbb{d}^1\boldsymbol{\eta}_\perp$: see [34, 7] for similar decompositions in non-conservative formulations.

Remark 7. The present derivation, from the general formulas (55), (57) and (58), of the linear perturbation equations for spherically-symmetric radial basic flows could be transposed to the case of cylindrical symmetry without raising any substantial difficulty.

A.3.3. Helmholtz decomposition of the transverse motion perturbation

By virtue of Helmholtz's theorem (*e. g.* see [36]), the transverse Lagrangian displacement perturbation field, $\mathbb{d}^1\boldsymbol{\eta}_\perp$, is entirely determined by the knowledge of the pair $(\mathrm{div}_\perp\, \mathbb{d}^1\boldsymbol{\eta}_\perp, \mathbf{rot}_\perp\, \mathbb{d}^1\boldsymbol{\eta}_\perp)$ through the potential Ξ and the stream function $\boldsymbol{\Psi} = \Psi^1\boldsymbol{\eta}_1$ which enter the decomposition

$$\mathbb{d}^1\boldsymbol{\eta}_\perp = \mathbf{grad}_\perp\, \Xi + \mathbf{rot}_\perp\, \boldsymbol{\Psi},$$

and are solutions of, respectively,

$$\Delta_\perp\Xi = \mathrm{div}_\perp\, \mathbb{d}^1\boldsymbol{\eta}_\perp, \qquad \text{and} \qquad \mathbf{rot}_\perp(\mathbf{rot}_\perp\, \boldsymbol{\Psi}) = \mathbf{rot}_\perp\, \mathbb{d}^1\boldsymbol{\eta}_\perp, \quad (69)$$

where, by definition,

$$\Delta_\perp X = \mathrm{div}_\perp(\mathbf{grad}_\perp\, X), \qquad \mathbf{rot}_\perp\, \boldsymbol{X} = \frac{1}{J_{\boldsymbol{\eta}}}\big[(\nabla_2 X_3 - \nabla_3 X_2)\boldsymbol{\eta}_1 + \nabla_3 X_1\boldsymbol{\eta}_2 - \nabla_2 X_1\boldsymbol{\eta}_3\big]. \quad (70)$$

We have then

PROPOSITION 8. *The motion linear perturbations, solutions of Eqs.* (65)*, are determined, up to solenoidal transverse motions satisfying the conditions*

$$\mathbb{d}^0 A\,\partial_t\,\mathbb{d}^1\theta = \mathrm{cst}, \qquad \mathbb{d}^0 A\,\partial_t\,\mathbb{d}^1\varphi = \mathrm{cst}, \tag{71}$$

by the solutions $\big(\mathbb{d}^1\tau,\ \mathbb{d}^1u^1,\ \mathbb{d}^1\Omega,\ \mathbb{d}^1e,\ \mathbb{d}^1r,\ \mathbb{d}^1\Theta\big)$ *of the system of equations*

$$\partial_t\,\mathbb{d}^1\tau - \partial_m\big(\mathbb{d}^0A\ \mathbb{d}^1u^1\big) - \mathbb{d}^0\tau\ \mathbb{d}^1\Omega - \partial_m\big(\mathbb{d}^1A\ \mathbb{d}^0u^1\big) - \partial_m\big(\mathbb{d}^0A\ \mathbb{d}^0u^1\big)\ \mathbb{d}^1\Theta = 0, \tag{72a}$$

$$\begin{aligned}\partial_t\,\mathbb{d}^1u^1 + \partial_m\big(\mathbb{d}^0A\ \mathbb{d}^1p\big) + \partial_m\big(\mathbb{d}^1A\ \mathbb{d}^0p\big) + \partial_m\big(\mathbb{d}^0A\ \mathbb{d}^0p\big)\ \mathbb{d}^1\Theta&\\ - \mathbb{d}^1p\,\partial_m\,\mathbb{d}^0A - \mathbb{d}^0p\,\big(\partial_m\,\mathbb{d}^1A + \partial_m\,\mathbb{d}^0A\ \mathbb{d}^1\Theta\big) = 0,&\end{aligned} \tag{72b}$$

$$\partial_t\big(\mathbb{d}^0A\ \mathbb{d}^1\Omega\big) + \mathbb{d}^0A\,\Big(\mathbb{d}^0\tau\,\Delta_\perp\,\mathbb{d}^1p + \Big[\mathbb{d}^0p\,\partial_m\,\mathbb{d}^0A - \partial_m\big(\mathbb{d}^0A\ \mathbb{d}^0p\big)\Big]\,\Delta_\perp\,\mathbb{d}^1r\Big) = 0, \tag{72c}$$

$$\begin{aligned}\partial_t\,\mathbb{d}^1e + \partial_m\big[\mathbb{d}^0A\ \mathbb{d}^1(p\,u^1)\big] + \mathbb{d}^0\tau\ \mathbb{d}^0p\ \mathbb{d}^1\Omega + \partial_m\big(\mathbb{d}^1A\ \mathbb{d}^0p\ \mathbb{d}^0u^1\big)&\\ +\partial_m\big(\mathbb{d}^0A\ \mathbb{d}^0p\ \mathbb{d}^0u^1\big)\ \mathbb{d}^1\Theta = 0,&\end{aligned} \tag{72d}$$

$$\partial_t\,\mathbb{d}^1r = \mathbb{d}^1u^1, \qquad \partial_t\,\mathbb{d}^1\Theta = \mathbb{d}^1\Omega, \tag{72e}$$

where

$$\mathbb{d}^1\Theta = \mathrm{div}_\perp\,\mathbb{d}^1\boldsymbol{\eta}_\perp, \qquad \mathbb{d}^1\Omega = \mathrm{div}_\perp\,\mathbb{d}^1\boldsymbol{u}_\perp, \tag{73}$$

denote, repectively, the dilatation *and* expansion *of the transverse motion linear perturbation.*

Proof. The differential equations (72c) and $\partial_t\,\mathbb{d}^1\Theta = \mathbb{d}^1\Omega$ of Eq. (72e) satisfied by the irrotational part, $\mathbf{grad}_\perp\,\Xi$, of the transverse motion perturbation, stem, for the latter, from Eq. (65e) and the fact that

$$\frac{d}{dt}\Big[\big(\partial_{\eta^i}\ln J_{\boldsymbol{\eta}}\big)\big|_{\mathbb{d}^0\boldsymbol{\eta}}\Big] = 0, \quad i \neq 1,$$

which results from Eq. (67), and, for the former, from applying $\mathrm{div}_\perp$ to Eq. (65c). In doing so, use is made of the equality

$$\mathrm{div}_\perp\left\{\frac{d}{dt}\Big[\big(g_{kk}|_{\mathbb{d}^0\boldsymbol{\eta}}\ \mathbb{d}^1u^k\big)_{k=i}\Big]\boldsymbol{\eta}^i\right\}_{i\neq1} = \frac{1}{J_{\boldsymbol{\eta}}|_{\mathbb{d}^0\boldsymbol{\eta}}}\,\frac{d}{dt}\big(J_{\boldsymbol{\eta}}|_{\mathbb{d}^0\boldsymbol{\eta}}\ \mathbb{d}^1\Omega\big) = \frac{1}{\mathbb{d}^0A}\,\partial_t\big(\mathbb{d}^0A\ \mathbb{d}^1\Omega\big),$$

which follows from the expression of the transverse divergence of a vector field, as provided by Eqs. (43) and (63), and the property

$$\frac{d}{dt}\,\big(J_{\boldsymbol{\eta}}\,g^{ii}\big)\big|_{\mathbb{d}^0\boldsymbol{\eta}} = 0, \quad i \neq 1,$$

a consequence of the fact that the quantities $J_{\boldsymbol{\eta}}\,g^{ii} = J_{\boldsymbol{\eta}}/g_{ii}$, $i \neq 1$, are independent of r.

Regarding the solenoidal part of the transverse motion perturbation, the evolution equation for $\mathbf{rot}_\perp\,\mathbb{d}^1\boldsymbol{\eta}_\perp$, as deduced from considering $\mathbf{rot}_\perp$ applied to Eq. (65c), takes the simple form of

$$\partial_t\,\Big[J_{\boldsymbol{\eta}}|_{\mathbb{d}^0\boldsymbol{\eta}}\ \partial_t\big(\mathbf{rot}_\perp\,\mathbb{d}^1\boldsymbol{\eta}_\perp\big)\Big] = \mathbf{0},$$

thanks to the independence of the quantities g_{ii}/r^2, $i \neq 1$, and $r^2/J_{\boldsymbol{\eta}}$ with respect to r. This last equation implies that the solenoidal part of the transverse motion perturbation, or $\mathbf{rot}_\perp\,\boldsymbol{\Psi}$, is such that its angular velocities, say $\partial_t\,\mathbb{d}^1\theta$ and $\partial_t\,\mathbb{d}^1\varphi$, satisfy the relations (71): see [7]. Hence, such a motion is entirely defined by its initial angular velocities and the basic flow motion. Moreover, since this solenoidal motion is absent from the other linear perturbation equations, namely Eqs. (65a), (65b), (65d), (66), and (72c), it may be treated independently from the rest of the flow perturbation, hence reducing the overall linear perturbation problem to the sole consideration of system (72). ∎

A.3.4. Spherical harmonics decomposition

Equations (60), (66) and (72) being linear in the unknowns $\big(\mathbb{d}^1\tau,\, \mathbb{d}^1u^1,\, \mathbb{d}^1\Omega,\, \mathbb{d}^1e,\, \mathbb{d}^1r,\, \mathbb{d}^1\Theta\big)$, one customarily proceeds to a decomposition of the linear perturbations over the basis of spherical harmonics: *e. g.* see [7, 14, 24]. We thus introduce, for any linear perturbation $\mathbb{d}^1X$ involved in (72), the expansion

$$\mathbb{d}^1X\big(m, \mathbb{d}^0\theta, \mathbb{d}^0\varphi, t\big) = \sum_{l=0}^{\infty}\sum_{l'=-l}^{l} \widetilde{X}(m,t;l,l')\, P_l^{l'}\big(\cos\mathbb{d}^0\theta\big)\, \exp\big(\mathrm{i}\, l'\, \mathbb{d}^0\varphi\big), \tag{74}$$

where $P_l^{l'}$ stands for Legendre's function of the first kind (*e. g.* see [28]), and where the function of (m,t), $\widetilde{X}$, is referred to as the *modal component* of degree l and order l' of $\mathbb{d}^1X$. Substituting the above expansions in Eqs. (60), (66), (72) and making use of the spherical harmonics property

$$\Delta_\perp\Big[P_l^{l'}(\cos\theta)\, \exp(\mathrm{i}\, l'\, \varphi)\Big] = -\frac{l(l+1)}{r^2}\, P_l^{l'}(\cos\theta)\, \exp(\mathrm{i}\, l'\, \varphi),$$

yields, for each pair (l,l'), a set of 1D PDEs for the corresponding modal components which does not depend on l'. Hence, modal components of a given degree l but of different orders l' all satisfy the same set of equations, differences in their temporal evolutions being the sole consequences of variations in the modal component initial or boundary conditions. With the notation introduced in Eq. (74) for the fluid quantity perturbation modal components, and omitting, for simplicity, the symbol $\mathbb{d}^0$ in front of the basic flow quantities and the superscript 1 of the fluid particle radial velocity contravariant component (i. e. $u^1 \to u$), this set of modal component 1D PDEs can be recast as the system (2)–(4), along with Eqs. (5) and (6).

APPENDIX B: LINEARIZED SIMPLE RIEMANN SOLVER

Consider the 1D Lagrangian system of gas dynamics in slab symmetry, or

$$\partial_t\mathbf{U} + \partial_\mu[\mathbf{F}(\mathbf{U})] = \mathbf{0}, \tag{75}$$

with $d\mu = \rho\, dx$, $u = \partial_t x$, and the notations of (1). Conservative numerical schemes for this system may be constructed [19] upon associating to the Riemann problem made of Eq. (75), $\mu \in \mathbb{R}$ and $t > 0$, with initial conditions

$$\mathbf{U}(\mu, 0) = \begin{cases} \mathbf{U}_\mathsf{L}, & \mu < 0, \\ \mathbf{U}_\mathsf{R}, & \mu > 0, \end{cases} \tag{76}$$

the approximate linear Riemann problem

$$\partial_t\mathbf{U} + \mathbf{A}^*(\mathbf{U}_\mathsf{L}, \mathbf{U}_\mathsf{R})\, \partial_\mu\mathbf{U} = \mathbf{0}, \quad \mu \in \mathbb{R}, \quad t > 0, \tag{77}$$

with identical initial conditions (76), where $\mathbf{A}^*$ is the Roe-type matrix [19, Eq. 13]

$$\mathbf{A}^*(\mathbf{U}_\mathsf{L}, \mathbf{U}_\mathsf{R}) = \begin{pmatrix} 0 & -1 & 0 \\ a & b & c \\ a\,\Sigma u/2 & (\Sigma p + b\,\Sigma u)/2 & c\,\Sigma u/2 \end{pmatrix}, \tag{78}$$

whose coefficients a, b, c are subject to the relations [19, Eq. 14]

$$\begin{cases} a\,\Delta\tau + b\,\Delta u + c\,\Delta e = \Delta p, \\ b + c\,\Sigma u/2 = 0, \\ a - c\,\Sigma p/2 = -C^{*2}. \end{cases}$$

The existence of such a Roe-type matrix and thus of the approximate Riemann problem (76), (77), is not always guaranteed [19, Proposition 3]. Nevertheless the simple Riemann solver

$\mathbf{W}(\mu/t; \mathbf{U}_{\mathsf{L}}, \mathbf{U}_{\mathsf{R}})$ of Eqs. (15), (16) which corresponds to the exact solution of this approximate Riemann problem — when it exists — is always defined. This solver actually defines a Godunov-type scheme for system (75), the associated numerical flux being given by (12): see [19, Propositions 4 and 5].

Let us now turn to the linearization of the 1D Lagrangian system (75), that is

$$\partial_t \widetilde{\mathbf{U}} + \partial_\mu \left[\frac{d\mathbf{F}}{d\mathbf{U}}(\mathbf{U})\, \widetilde{\mathbf{U}} \right] = \mathbf{0}, \tag{79}$$

with $\widetilde{u} = \partial_t \widetilde{x}$ and the notations of (3). For the Riemann problem made of Eq. (75), $\mu \in \mathbb{R}$ and $t > 0$, with (76), and Eq. (79), $\mu \in \mathbb{R}$ and $t > 0$, with

$$\widetilde{\mathbf{U}}(\mu, 0) = \begin{cases} \widetilde{\mathbf{U}}_{\mathsf{L}}, & \mu < 0, \\ \widetilde{\mathbf{U}}_{\mathsf{R}}, & \mu > 0, \end{cases} \tag{80}$$

we introduce the solver $\widetilde{\mathbf{W}}(\mu/t; \mathbf{U}_{\mathsf{L}}, \mathbf{U}_{\mathsf{R}}, \widetilde{\mathbf{U}}_{\mathsf{L}}, \widetilde{\mathbf{U}}_{\mathsf{R}})$ as being the *linearization* of the simple Riemann solver (15), (16) where, in accordance with the definition of the Roe-type matrix (78), the wave speed C^* is taken to be a fixed parameter. This construction leads to the definitions of Eqs. (17), (18) and to the notion of *linearized simple Riemann solver.* With such a definition we have

PROPOSITION 9. *The linearized simple Riemann solver* (17), (18) *defines a Godunov-type scheme for system* (79). *The associated numerical flux is given by Eq.* (13).

Proof. Proving that the solver (17), (18) defines a Godunov-type scheme for system (79), amounts to showing that $\widetilde{\mathbf{W}}(\mu/t; \mathbf{U}_{\mathsf{L}}, \mathbf{U}_{\mathsf{R}}, \widetilde{\mathbf{U}}_{\mathsf{L}}, \widetilde{\mathbf{U}}_{\mathsf{R}})$ is consistent with the integral form of (79): *e. g.* see [19, Proposition 2]. This is easily done by checking that, given the definitions (3), (16)–(18), the consistency relation

$$\frac{d\mathbf{F}}{d\mathbf{U}}(\mathbf{U}_{\mathsf{R}})\, \widetilde{\mathbf{U}}_{\mathsf{R}} - \frac{d\mathbf{F}}{d\mathbf{U}}(\mathbf{U}_{\mathsf{L}})\, \widetilde{\mathbf{U}}_{\mathsf{L}} = -C^* \left[\widetilde{\mathbf{U}}_2 - \widetilde{\mathbf{U}}_1 \right] + C^* \left[\widetilde{\mathbf{U}}_4 - \widetilde{\mathbf{U}}_3 \right],$$

is satisfied.

This consistency relation being verified, the numerical flux associated to this linearized simple Riemann solver is inferred from applying the general definition of a simple Riemann solver numerical flux [19, Eq. (9)], whence

$$\widetilde{\mathbf{f}}(\mathbf{U}_{\mathsf{L}}, \mathbf{U}_{\mathsf{R}}, \widetilde{\mathbf{U}}_{\mathsf{L}}, \widetilde{\mathbf{U}}_{\mathsf{R}}) = \frac{1}{2} \left(\frac{d\mathbf{F}}{d\mathbf{U}}(\mathbf{U}_{\mathsf{L}})\, \widetilde{\mathbf{U}}_{\mathsf{L}} + \frac{d\mathbf{F}}{d\mathbf{U}}(\mathbf{U}_{\mathsf{R}})\, \widetilde{\mathbf{U}}_{\mathsf{R}} - C^* \left[\widetilde{\mathbf{U}}_2 - \widetilde{\mathbf{U}}_1 \right] - C^* \left[\widetilde{\mathbf{U}}_4 - \widetilde{\mathbf{U}}_3 \right] \right).$$

All calculations being made, this definition yields the expression (13). ∎

APPENDIX C: APPLICATION OF THE GEOMETRIC CONSERVATION LAW TO THE MODAL FLOW MOTION

The derivation of the expressions (20) and (21) of the approximants $\widetilde{A}_{j+1/2}^{n+1/2}$ and $\widetilde{\Theta}_j^{n+1/2}$, by means of the discrete formulation of the geometric (or mass) conservation law for the linearized flow motion modal component, comes as follows.

Approximant $\widetilde{A}_{j+1/2}^{n+1/2}$ Consider the conservation law for $\widetilde{\tau}$ in Eq. (2), or

$$\partial_t \widetilde{\tau} + \partial_m \big(-A\, \widetilde{u} \big) - \tau\, \widetilde{\Omega} + \partial_m \big(-\widetilde{A}\, u \big) + \partial_m \big(-A\, u \big)\, \widetilde{\Theta} = 0. \tag{81}$$

From the conservation law satisfied by τ (see Eq. 1), we get that

$$\tau\, \widetilde{\Omega} + \partial_m \big(A\, u \big)\, \widetilde{\Theta} = \partial_t \big(\tau\, \widetilde{\Theta} \big), \tag{82}$$

so that Eq. (81) may also be written as

$$\partial_t \widetilde{\tau} = \partial_m\big(A\,\widetilde{u}\big) + \partial_m\big(\widetilde{A}\,u\big) + \partial_t\big(\tau\,\widetilde{\Theta}\big),$$

i. e. the time-derivative of the mass conservation equation for the modal components (5). Integrating this very equation over $(m_{j-1/2}, m_{j+1/2}) \times (t_n, t_{n+1})$ and comparing it with the variation, between t_n and t_{n+1}, of Eq. (5) integrated over $(m_{j-1/2}, m_{j+1/2})$, leads to the equality

$$\int_{t_n}^{t_{n+1}} \big[A\,\widetilde{u} + \widetilde{A}\,u\big]_{j-1/2}^{j+1/2}\,dt = \big[A^{n+1}\,\widetilde{r}^{n+1}\big]_{j-1/2}^{j+1/2} - \big[A^n\,\widetilde{r}^n\big]_{j-1/2}^{j+1/2}.$$

Given the approximations introduced by the discrete equations (9), we conclude that the scheme thus defined is compatible with the above volume conservation if the relation

$$\Big[\Delta t_n\left(A^{n+1/2}\,\widetilde{u}^{*n} + \widetilde{A}^{n+1/2}\,u^{*n}\right) - \big[A\,\widetilde{r}\big]_n^{n+1}\Big]_{j-1/2}^{j+1/2} = 0, \tag{83}$$

holds whatever the values of Δt_n and of the cell size Δm_j, whence the equality

$$\Delta t_n\left(A_{j+1/2}^{n+1/2}\,\widetilde{u}^{*n}_{\;j+1/2} + \widetilde{A}_{j+1/2}^{n+1/2}\,u^{*n}_{\;j+1/2}\right) = \Big[A_{j+1/2}\,\widetilde{r}_{j+1/2}\Big]_n^{n+1},$$

whatever j. Upon replacing $r_{j+1/2}^{n+1}$, $A_{j+1/2}^{n+1/2}$ and $\widetilde{r}_{j+1/2}^{n+1}$ by their respective definitions — namely Eqs. (8b), (19) and (9d) — in this last equation, one obtains the correct definition (20) of $\widetilde{A}_{j+1/2}^{n+1/2}$.

Approximant $\widetilde{\Theta}_j^{n+1/2}$ The above result has been obtained regardless of the discrete approximations which may have been chosen for the left-hand side of Eq. (82). In other words, in writing down (83) we implicitly require that the discrete formulation of (82) is verified by the present scheme definition. Letting $\tau_j^n\,\widetilde{\Theta}_j^n$, for any n, be the approximation of the cell-averaged value

$$\frac{1}{\Delta m_j}\int_{m_{j-1/2}}^{m_{j+1/2}} \big(\tau\,\widetilde{\Theta}\big)^n\,dm,$$

the discrete form of (82), given the approximation (22), corresponds then to the equality

$$\Delta m_j\,\big[\tau_j\,\widetilde{\Theta}_j\big]_n^{n+1} = \Delta t_n\left(\tau_j^n\,\widetilde{\Omega}_j^n + \Big[A^{n+1/2}\,u^{*n}\Big]_{j-1/2}^{j+1/2}\,\widetilde{\Theta}_j^{n+1/2}\right), \tag{84}$$

which relates the modal cell-volume transverse dilatation to the modal transverse-expansion and basic radial motions. Making use of the equation for τ_j^{n+1} in (8a) and of the relation (9e), the above equation immediately leads to the proper definition (21) of $\widetilde{\Theta}_j^{n+1/2}$.

APPENDIX D: NUMERICAL STABILITY OF THE MODAL COMPONENT SCHEME

A numerical stability analysis of the modal component scheme (9) in the most general case of arbitrary basic flows can hardly be performed. However, under the restrictive assumption of a uniform and constant basic flow with planar symmetry, a von Neumann stability analysis may be carried out. This analysis aims at obtaining a local stability criterion of practical use in the general case, the validity of this criterion having to be assessed from numerical experiments.

Under the above assumption, the space-discretized formulation of (2), (4a) with the definitions of (9)–(13) reduces to

$$\begin{aligned}
\partial_t \widetilde{\mathbf{U}}_j &= -\frac{1}{\Delta\mu_j}\Big[\widetilde{\mathbf{F}}\big(\mathbf{U}^0, \widetilde{\mathbf{U}}\big)\Big]_{j-1/2}^{j+1/2} - \tau^0\,\widetilde{\mathbf{F}}^{\perp}\big(\mathbf{U}^0, \widetilde{\Omega}\big)_j,\\
\partial_t \widetilde{\Omega}_j &= -\mathrm{w}\,\tau^0\,\widetilde{p}_j,
\end{aligned} \tag{85}$$

where $\Delta\mu_j$ is the Lagrangian mass-coordinate step in planar symmetry, $\mathbf{U}^0$ denotes the uniform and constant basic flow state, $\widetilde{\mathbf{U}}$ stands for the linear perturbation Fourier component of wavenumber $k_\perp$, and $\mathrm{w} = -k_\perp^2$. For a piecewise constant reconstruction of $(\widetilde{\mathbf{U}}_j)$, this system is equivalent to

$$\partial_t \widetilde{\mathbf{V}}_j = -\frac{1}{\Delta\mu_j}\,\mathbf{A}^+_{\mathbf{V}}\,\big[\widetilde{\mathbf{V}}\big]_{j-1}^{j} - \frac{1}{\Delta\mu_j}\,\mathbf{A}^-_{\mathbf{V}}\,\big[\widetilde{\mathbf{V}}\big]_{j}^{j+1} - \mathbf{B}_{\mathbf{V}}\,\widetilde{\mathbf{V}}_j,$$

with $\widetilde{\mathbf{V}} = \big(\widetilde{p} - C^0\,\widetilde{u},\ \widetilde{p} + {C^0}^2\,\widetilde{\tau},\ \widetilde{\Omega},\ \widetilde{p} + C^0\,\widetilde{u}\big)^\top$, and

$$\mathbf{A}^+_{\mathbf{V}} = \begin{pmatrix} 0 & 0 & 0 & 0 \\ 0 & 0 & 0 & 0 \\ 0 & 0 & 0 & 0 \\ 0 & 0 & 0 & C^0 \end{pmatrix}, \quad \mathbf{A}^-_{\mathbf{V}} = \begin{pmatrix} -C^0 & 0 & 0 & 0 \\ 0 & 0 & 0 & 0 \\ 0 & 0 & 0 & 0 \\ 0 & 0 & 0 & 0 \end{pmatrix}, \quad \mathbf{B}_{\mathbf{V}} = \begin{pmatrix} 0 & 0 & \tau^0 {C^0}^2 & 0 \\ 0 & 0 & 0 & 0 \\ \frac{\mathrm{w}}{2}\tau^0 & 0 & 0 & \frac{\mathrm{w}}{2}\tau^0 \\ 0 & 0 & \tau^0 {C^0}^2 & 0 \end{pmatrix}.$$

Assuming a uniform spatial grid of cell-size $\Delta\mu$, the discrete Fourier representation of this system may be written as

$$\partial_t \widetilde{\boldsymbol{\mathcal{V}}}_\phi = \nu\,\mathbf{H}_\phi\,\widetilde{\boldsymbol{\mathcal{V}}}_\phi, \tag{86}$$

where $\widetilde{\boldsymbol{\mathcal{V}}}_\phi$ stands for the harmonic component of $(\widetilde{\mathbf{U}}_j)$, of phase angle ϕ $(-\pi < \phi < \pi)$; $\nu = C^0/\Delta\mu$ is the frequency of cell-crossing longitudinal sound waves; and $\mathbf{H}_\phi$ is a 4×4 matrix of characteristic polynomial

$$\det(\mathbf{H}_\phi - Z\,\mathbf{I}) = Z\,\mathrm{P}^3_\phi(Z),$$

with $\mathrm{P}^3_\phi(Z)$ a real coefficient cubic polynomial. This polynomial which depends — apart from the phase angle ϕ — on a single parameter, namely the number of grid cells per transverse wavelength, or

$$\mathfrak{N} = 2\pi\big(\sqrt{|\mathrm{w}|}\,\Delta x\big)^{-1} = \lambda_\perp/\Delta x, \tag{87}$$

has its roots of bounded real parts, in effect

$$-2 \le \mathrm{Re}Z \le 0, \tag{88}$$

and its complex conjugate roots of imaginary parts such that

$$|\mathrm{Im}Z| \sim 2\pi\,\mathfrak{N}^{-1},$$

as $\mathfrak{N} \to 0^+$. Computing vanishing transverse wavelength perturbations is therefore a matter of handling arbitrary large imaginary growth rates, rather than dealing with a source-term stiffness of some sort as it is stated in [31, Sec. 3.2]. In particular, the first-order explicit schemes previously proposed in [39, 11, 22, 30, 13] inevitably become unstable as the computational grid gets coarser with respect to the perturbation transverse wavelengths (i. e. as $\mathfrak{N} \to 0^+$). This pitfall which could be circumvented in planar symmetry by a grid refinement, is unavoidable in spherical symmetry where fluid systems which include the center of symmetry necessarily involve perturbations of arbitrarily small transverse wavelength. On the other hand, the third-order explicit Runge–Kutta time-integrator based scheme described in [13] presents the desired stability property provided that an effective stability criterion is furnished.

Practical stability criterion Given the domain of stability of explicit third-order non-degenerate Runge–Kutta schemes (*e. g.* see [40, Fig. 4.16]), we consider, following [6, Sec. 4.2], the stability sub-domain

$$(\Delta t\,\nu\,\mathrm{Re}Z/\beta_1)^2 + (\Delta t\,\nu\,\mathrm{Im}Z/\beta_2)^2 \le 1, \tag{89}$$

for the differential equation (86), where the coefficients

$$\beta_1 = 1 - \big(4 + \sqrt{17}\big)^{-1/3} + \big(4 + \sqrt{17}\big)^{1/3}, \quad \beta_2 = \sqrt{3},$$

are the intersections of the exact stability domain boundary with the real and imaginary axes [40, Table 4.8]. By means of Cardano's formulas for the roots of a cubic, explicit bounds — uniform in ϕ — on the imaginary part amplitudes of the roots of $\mathrm{P}^3_\phi(Z)$ may be obtained. With the help of such a bound, say $\widehat{\mathrm{Im}Z}(\mathfrak{N})$, and of the inequality (88), we infer from (89) the expression for a local critical time step as

$$\Delta t_{\mathrm{w}}{}^n_j = \left(\widehat{\nu}^n_j \sqrt{(2/\beta_1)^2 + \left(\widehat{\mathrm{Im}Z}(\mathfrak{N}^n_j)/\beta_2\right)^2} \right)^{-1}, \tag{90}$$

where $\widehat{\nu}^n_j$ is defined to be

$$\widehat{\nu}^n_j = \tau^n_j \, \widehat{C}^n_j / \Delta x^n_j, \quad \text{with} \quad \widehat{C}^n_j = \max_{|j-i| \leq \Delta j} \left\{ C^{*n}_{i-1/2}, C^n_i, C^{*n}_{i+1/2} \right\}, \tag{91}$$

for some integer constant Δj, $\mathfrak{N}^n_j$ being the cell value of (87), and replace the stability condition (89) relevant to uniform constant basic flows by the condition

$$\Delta t_n \leq \min_j \Delta t_{\mathrm{w}}{}^n_j, \tag{92}$$

for arbitrary basic flows. The above form (90) of critical time step is not uncommon for gas dynamics linear perturbation explicit schemes: cf. [24, Eq. (12)] and [6, Eqs. (44) & (45)].

The behavior of this critical time step Δt_{w} as a function of the number of cells per transverse wavelength $\mathfrak{N}$ is represented in Figure 8 under the form of the Courant number $\widehat{\nu}\,\Delta t_{\mathrm{w}}$. In particular, this Courant number appears to be within 0.1% of its maximum value ($\max(\widehat{\nu}\,\Delta t_{\mathrm{w}}) \simeq 0.8678$) as soon as $\mathfrak{N} \geq 100$, and within 10% for $\mathfrak{N} \geq 10$, while falling below 0.26 for $\mathfrak{N} \leq 1$. Hence, by comparison with the basic-flow explicit scheme Courant number ($\nu\,\Delta t = 1$), the overhead associated to the use of the proposed flow modal-component explicit scheme is all the most acceptable for a reasonable transverse wavelength sampling (i. e. for $\mathfrak{N} \geq 10$).

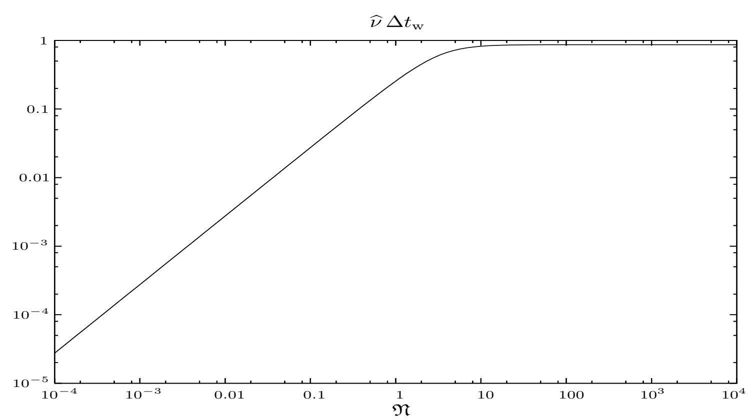

FIG. 8 Plot of the Courant number $\widehat{\nu}\,\Delta t_{\mathrm{w}}$, as defined after Eq. (90), vs the number of cells per transverse wavelength $\mathfrak{N}$.

Numerical tests The above time-step constraint (92) has been found to furnish a sufficient stability condition when computing the propagation of linear perturbation acoustic plane waves about a uniform static equilibrium basic state. The corresponding computations were performed with the spatially first-order scheme (9) coupled to the third-order Runge–Kutta time-integrator of [43], over more than 128 wave-periods, for a computational domain with periodic boundary conditions, and for wavevectors $(k_x, k_\perp)$ such that

$$(k_x\,\Delta x, k_\perp\,\Delta x) = \left(4^{q_1-5}\,\pi, 4^{q_2-5}\,\pi\right), \quad 0 \leq q_1 \leq 5, \quad \text{and} \quad 0 \leq q_2 \leq 10,$$

thus sampling the range $1/512 \leq \mathfrak{N} \leq 2048$.

The case of a nonuniform basic flow has also been considered by computing a rippled planar shock wave solution [37] at a given transverse wavenumber, $k_\perp = 10^3$, for different spatial grid steps. Results (see Figure 9) indicate that the proposed scheme (9), both in its spatially first-order and MUSCL-type variants, is stable with the third-order Runge-Kutta integrator [43] under condition (92), with $\Delta j = 0$ or $\Delta j \neq 0$ in (91), for initial grid resolutions as low as $\mathfrak{N}^0 = 2$. Such low values of $\mathfrak{N}$ should however be avoided as they lead to high levels of errors (cf. the curves $\mathfrak{N}^0 = 3.0$ and $\mathfrak{N}^0 = 2.0$ in Figure 9). (These levels may be reduced, only to a certain extent, by decreasing the time step.) In fact, since at least two points are needed to capture a periodic signal, there is no point in considering spatial discretization grid with $\mathfrak{N}_j^n < 2$, whence the minimum grid requirement: $\mathfrak{N}_j^n \geq 2$.

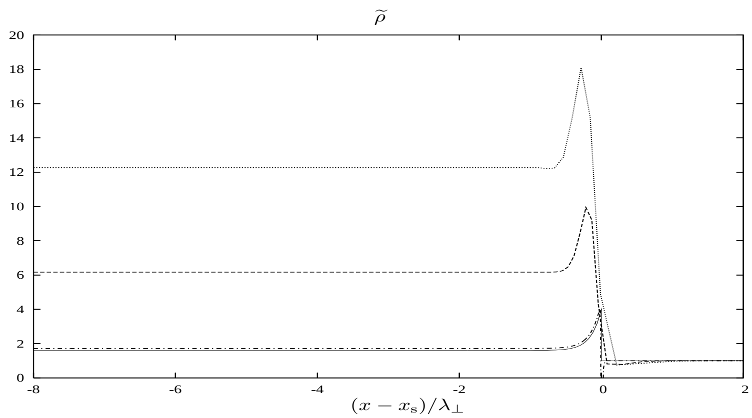

FIG. 9 Rippled planar shock wave. Profiles of the density modal component $\widetilde{\rho}$ plotted in the shock-front reference frame as functions of the x coordinate normalized by the perturbation transverse wavelength $\lambda_\perp$. Results obtained with the spatially first-order scheme under condition (92), with $\Delta j = 5$ in (91), for initial values of the number of cells per transverse wavelength of $\mathfrak{N}^0 = 2.0$ (dotted line), $\mathfrak{N}^0 = 3.0$ (dashed line) and $\mathfrak{N}^0 = 50.3$ (dash-dotted line). The exact steady solution [37] in this reference frame is also given (solid line). The corresponding basic flow is a planar shock wave traveling from left to right as computed for the Noh test case conditions [38]. This shock wave which is constantly fed with an upstream entropy ripple of wavenumber parallel to the front ($\widetilde{\rho} = 1$ for $x > x_s$), induces a downstream evanescent acoustic mode (exponential profile for $x < x_s$): cf. [37]. Computed results are here shown by the time the shock front has traveled over 941 transverse wavelengths after the upstream perturbation has been switched on.

REFERENCES

[1] G. Birkhoff. Note on Taylor instability. *Quart. Appl. Math.*, 12:306–309, 1954.

[2] V. Bjerknes, J. Bjerknes, H. Solberg, and T. Bergeron. *Hydrodynamique physique avec applications à la météorologie dynamique.* Presses Universitaires de France, Paris, 1934. (French edition of *Physikalische hydrodynamik.* Springer, Berlin, 1933.).

[3] D. L. Book and I. B. Bernstein. Fluid instabilities of a uniformly imploding ablatively driven shell. *J. Plasma Physics*, 23:521–533, 1980.

[4] C. Boudesocque-Dubois and J.-M. Clarisse. Investigation of linear perturbation growth in a planar ablation flow. In O. N. Krokhin, S. Y. Gus'kov, Y. A. Merkul'ev, editor, *ECLIM 2002: 27th European Conference on Laser Interaction with Matter*, volume 5228 of *Proceedings of SPIE*, pages 172–183. SPIE, 2003.

[5] C. Boudesocque-Dubois and J.-M. Clarisse. Traitement numérique des équations de la dynamique des gaz avec conduction non linéaire dans le code de perturbations SILE$\mathfrak{X}$. Internal Report, CEA, 2003. (in French, published as Technical Report CEA-R-6137, CEA, 2007).

[6] C. Boudesocque-Dubois, J.-M. Clarisse, and S. Gauthier. A spectral Chebyshev method for linear stability analysis of one-dimensional exact solutions of gas dynamics. *J. Comp. Phys.*, 184:592–618, 2003.

[7] L. Brun and B. Sitt. Approche lagrangienne du problème des instabilités hydrodynamiques d'une implosion à symétrie plane ou sphérique. Technical Report CEA-R-5012, CEA, 1979.

[8] V. Ya. Bukharova, G. A. Grishina, and O. M. Zotova. Code for computing small perturbations in gas dynamics problems. *VANT. Ser. Met. i progr. chisl. resh. zad. mat. fiziki*, 3:22–30, 1986. (in Russian).

[9] D. S. Butler. Stability of converging cylindrical and spherical shock waves. Technical Report 18/56, ARDE, 1956.

[10] R. F. Chisnell. An analytic description of converging shock waves. *J. Fluid Mech.*, 354:357–375, 1998.

[11] J.-M. Clarisse. Pertubation linéaire d'écoulements à symétrie sphérique : schéma décentré d'ordre 1 pour les équations de la dynamique des gaz en variables de Lagrange. Internal Report, CEA, 2001. (in French, published as Technical Report CEA-R-6138, CEA, 2007).

[12] J.-M. Clarisse, C. Boudesocque-Dubois, J.-P. Leidinger, and J.-L. Willien. A linear perturbation computation method applied to hydrodynamic instability growth predictions in ICF targets. *J. Phys. IV France*, 133:201–204, 2006.

[13] J.-M. Clarisse, S. Jaouen, and P.-A. Raviart. A Godunov-type method in Lagrangian coordinates for computing linearly-perturbed planar-symmetric flows of gas dynamics. *J. Comp. Phys.*, 198:80–105, 2004.

[14] J. P. Cox. *Theory of stellar pulsation.* Princeton Series in Astrophysics. Princeton University Press, 1980.

[15] B. Després. Inégalités entropiques pour un solveur de type Lagrange + convection des équations de l'hydrodynamique. Technical Report CEA-N-2822, CEA, 1997. (in French).

[16] B. Després. Lagrangian systems of conservation laws. Invariance properties of Lagrangian systems of conservation laws, approximate Riemann solvers and the entropy condition. *Numer. Math.*, 89:99–134, 2001.

[17] P. G. Drazin and W. H. Reid. *Hydrodynamic stability.* Cambridge University Press, Cambridge, U.K., 1981.

[18] A. K. Evans. Instability of converging shock waves and sonoluminescence. *Phys. Rev. E*, 54:5004–5011, 1996.

[19] G. Gallice. Positive and entropy stable Godunov-type schemes for gas dynamics and MHD equations in Lagrangian or Eulerian coordinates. *Numer. Math.*, 94:673–713, 2003.

[20] J. H. Gardner, D. L. Book, and I. B. Bernstein. Stability of imploding shocks in the CCW approximation. *J. Fluid Mech.*, 114:41–58, 1982.

[21] E. Godlewksi and P.-A. Raviart. *Numerical approximation of hyperbolic systems of conservation laws.* Applied Mathematical Sciences. Springer-Verlag, New-York, 1996.

[22] E. Godlewski, M. Olazabal, and P.-A. Raviart. A Godunov-type method for studying the linearised stability of a flow. Application to the Richtmyer-Meshkov instability. In E. F. Toro, editor, *Godunov methods: theory and applications*, pages 377–397. Kluwer Academic/Plenum Publishers, 2001.

[23] E. Godlewski and P.-A. Raviart. The linearized stability of solutions of nonlinear hyperbolic systems of conservation laws. A general numerical approach. *Math. Comp. Simulation*, 50:77–95, 1999.

[24] G. A. Grishina. Linear approximation method in gas dynamics problem numerical computations. Technical Report 121, USSR Academy of Sciences IAM, Moscow, 1980. (in Russian).

[25] S. W. Haan, M. C. Hermann, T. R. Dittrich, A. J. Fetterman, M. M. Marinak, D. H. Munro, S. M. Pollaine, J. D. Salmonson, G. L. Strobel, and L. J. Suter. Increasing robustness of indirect drive capsule designs against short wavelength hydrodynamic instabilities. *Phys. Plasmas*, 312:056316, 2005.

[26] F. Hattori, H. Takabe, and K. Mima. Rayleigh-Taylor instability in a spherically stagnating system. *Phys. Fluids*, 29:1719–1724, 1986.

[27] D. B. Henderson and R. L. Morse. Symmetry of laser-driven implosions. *Phys. Rev. Lett.*, 32:355–358, 1974.

[28] E. N. Hobson. *The theory of spherical and ellipsoidal harmonics.* Cambridge Univ. Press, 1931.

[29] S. H. R. Hosseini and K. Takayama. Implosion of a spherical shock wave reflected from a spherical wall. *J. Fluid Mech.*, 530:223–239, 2005.

[30] S. Jaouen. *Étude mathématique et numérique de stabilité pour des modèles hydrodynamiques avec transition de phase.* PhD thesis, Université Paris 6, 2001.

[31] S. Jaouen. A purely Lagrangian method for computing linearly-perturbed flows in spherical geometry. *J. Comp. Phys.*, 225:464–490, 2007.

[32] R. E. Kidder. Laser-driven compression of hollow shells: power requirements and stability limitations. *Nucl. Fusion*, 16:3–14, 1976.

[33] P. Ledoux and T. Walraven. Variable stars. In *Handbuch der Physik*, pages 353–604. Springer, Berlin, 1958.

[34] R. L. McCrory, R. L. Morse, and K. A. Taggart. Growth and saturation of instability of spherical implosions driven by laser or charged particle beams. *Nucl. Sci. Eng.*, 64:163–176, 1977.

[35] J. Morice and S. Jaouen. Perturbations linéaires d'écoulements monodimensionnels à géométries plane, cylindrique et sphérique. Technical Report CEA-R-6040, CEA, 2003. (in French).

[36] P. M. Morse and H. Feshbach. *Methods of theoretical physics.* McGraw Hill, 1953.

[37] D. H. Munro. Rippled shock front solutions for testing hydrodynamic stability simulations. *Phys. Fluids B*, 1:134–141, 1989.

[38] W. F. Noh. Errors for calculations of strong shocks using an artificial viscosity and an artificial heat flux. *J. Comp. Phys.*, 72:78–120, 1987.

[39] M. Olazabal. *Modélisation numérique de problèmes de stabilité linéarisée. Application aux équations de la dynamique des gaz et de la MHD idéale.* PhD thesis, Université Paris 6, 1998.

[40] R. Peyret. *Spectral methods for incompressible viscous flow*, volume 148 of *Applied mathematical sciences*. Springer, New-York, 2002.

[41] L. Sedov. *Mécanique des milieux continus*. Mir, Moscow, French edition, 1975.

[42] J. N. Shiau, E. B. Goldman, and C. I. Weng. Linear stability analysis of laser-driven spherical implosions. *Phys. Rev. Lett.*, 32:352–355, 1974.

[43] C.-W. Shu and S. Osher. Efficient implementation of essentially non-oscillatory shock capturing schemes. *J. Comp. Phys.*, 77:439–471, 1988.

[44] B. Sitt and N. Wilke. Etude de l'instabilité linéaire du choc sphérique convergent. Technical Report CEA-R-5054, CEA, 1980.

[45] R. W. Smith. AUSM(ALE): a geometrically conservative arbitrary Lagrangian-Eulerian flux splitting scheme. *J. Comp. Phys.*, 150:268–286, 1999.

[46] P. D. Thomas and C. K. Lombard. Geometric conservation law and its application to flow computations on a moving grid. *AIAA J.*, 17:1030–1037, 1979.

[47] E. F. Toro. *Riemann solvers and numerical methods for fluid dynamics: a practical introduction*. Springer, Berlin, 2nd edition, 1999.

[48] G. B. Whitham. *Linear and nonlinear waves*. Wiley-Interscience, New-York, 1974.